UNIVERSIDADE ESTADUAL PAULISTA
"JÚLIO DE MESQUITA FILHO"
CAMPUS DE GUARATINGUETÁ

HENRIQUE DE ALMEIDA SILVA MASCALHUSK BERNARDO LEITE

Effect of deformed nuclei in hydrodynamic evolution and bulk observables :

Guaratinguetá
2022

Henrique de Almeida Silva Mascalhusk Bernardo Leite

Effect of deformed nuclei in hydrodynamic evolution and bulk observables :

Dissertação apresentada à Faculdade de Engenharia do Campus de Guaratinguetá, Universidade Estadual Paulista, para obtenção do título de Mestre em Física.

Orientador: Profº Dr. Wei-Liang Qian
Coorientador:

Guaratinguetá
2022

Leite, Henrique de Almeida Silva Mascalhusk Bernardo
L533e Effect of deformed nuclei in hydrodynamic evolution and bulk observables / Henrique de Almeida Silva Mascalhusk Bernardo Leite – Guaratinguetá, 2022.
81 f : il.
Bibliografia: f. 80-81

Dissertação (Mestrado) – Universidade Estadual Paulista, Faculdade de Engenharia de Guaratinguetá, 2022.

Orientador: Prof. Dr. Wei-Liang Qian

1. Colisões (Física). 2. Ions. 3. Hidrodinâmica. I. Título.

CDU 539.17

Luciana Máximo
Bibliotecária/CRB-8 3595

unesp *UNIVERSIDADE ESTADUAL PAULISTA*
CAMPUS DE GUARATINGUETÁ

HENRIQUE DE ALMEIDA SILVA MASCALHUSK BERNARDO LEITE

ESTA DISSERTAÇÃO FOI JULGADA ADEQUADA PARA A OBTENÇÃO DO TÍTULO DE
"MESTRADO EM FÍSICA"

PROGRAMA: FÍSICA
CURSO: MESTRADO

APROVADA EM SUA FORMA FINAL PELO PROGRAMA DE PÓS-GRADUAÇÃO

Prof. Dr. Ernesto Vieira Neto
Coordenador

BANCA EXAMINADORA:

Prof. Dr. WEILIANG QIAN
Orientador - UNESP
participou por videoconferência

Prof. Dr. ROGÉRIO TEIXEIRA CAVALCANTI
UNESP
participou por videoconferência

Prof. Dr. KAI LIN
China University of Geosciences
participou por videoconferência

Janeiro *de 2022*

DADOS CURRICULARES

HENRIQUE DE ALMEIDA SILVA MASCALHUSK BERNARDO LEITE

NASCIMENTO	28/05/1995 - São Sebastião / São Paulo
FILIAÇÃO	Luiz Bernardo Leite Filho Vilma de Almeira Ribeiro Leite
2019 / 2022	Mestrado em Física Universidade Estadual Paulista
2014 / 2019	Bacharel em Física com Ênfase em Física Computacional Universidade Federal Fluminense

This study was financed in part by the Coordenação de Aperfeiçoamento de Pessoal de Nível Superior-Brasil (CAPES) - Finance Code 001.

ABSTRACT

This work involves a numerical study of relativistic heavy-ion collisions based on hydrodynamic models. It is well-known that the collision process between two nuclei in the relativistic heavy ion collider (RHIC) gives rise to a fireball with high energy density and temperature. The latter furnishes an extreme condition, feasible to accommodate an asymptotic form of matter under the strong interaction, namely, the quark-gluon plasma (QGP). Some recent developments indicated that the initial geometry of nuclei may lead to relevant effects on the experimental observables. Motivated by such considerations, the goal of our ongoing study is to analyze the relation between the initial geometry and the final state observables. This is implemented by carrying out a systematic study for various types of nuclei, such as gold (Au) and uranium (U), subjected to different possible degrees of deformations. By evaluating the observables such as multiplicity spectra, fluctuations, collective flow, and correlations, one aims to tell whether the potential differences in these quantities suffice to distinguish the initial conditions. Results are presented and discussed.

KEYWORDS: Relativistic Heavy-ion Collisions. Quark Gluon Plasma. Initial Geometry. Elliptic Flow.

RESUMO

Esse trabalho envolve um estudo numérico em colisões relativísticas de íons pesados baseados em modelos hidrodinâmicos. Sabemos que o processo de colisão entre dois núcleos no colisor de ions pesados (RHIC) gera uma "*firebal*"com alta densidade de energia e temperatura. Essas condições extremas fornecem condições para acomodar de forma assintótica sob ação de interações fortes, sendo nomeada plasma de quarks e gluons (QGP). Alguns estudos recentes mostram que a geometria initial dos núcloe podem desempenhar efeitos relevantes nos observáveis experimentais. Motivados por estas considerações, o objetivo deste estudo é analizar a relação entre a geometria inicial e o estado final dos observáveis. Isto será realizado com de forma sistemática com diversos tipos de núclos, como gold (Au) e urânio (U), sujeitos a possíveis graus de deformações. Calculando-se os observáveis como o espectro de multiplicidade, flutuações, fluxo colletivo, e correlações, visamos descrever as potenciais diferenças nessas quantidades de acordo com as distintas condições iniciais. Resultados preliminares serão apresentados e discutidos.

PALAVRAS-CHAVE: Colisão Relativística de Íons pesados. Plasma de quarks e glúons. Geometria inicial. Fluxo elíptico.

LISTA DE ILUSTRAÇÕES

LISTA DE TABELAS

SUMÁRIO

1 INTRODUCTION

The relativistic heavy-ion collisions (RHIC) are a specific research area in physics that possesses an inter-disciplinary nature. On the theoretical side, among others, it involves subjects associated with quantum collision theory, quantum chromodynamics, relativistic hydrodynamics, thermodynamics and statistics, and relativistic kinetic theory. Regarding the energy scale, the relevant topics often reside on the interface between particle physics and high-energy nuclear physics (BHALERAO,).

We have an idea of atoms since ancient Greece, and until the revolution of the electron, nuclei and the establishment of the atomic model we didn't have a full comprehension about one of the most fundamental matter in our world, the atoms. After Rutherford proposed his atomic model in 1911, the science earned a new field or research, and allowed us to understand the components of atoms in a more fundamental way.

In this context, the science of particle physics surged, to carry information on the composition of the atoms. In particular, after '40s when the accelerators reached high energies and had become feasible, many types of particles were found such as pions by César Lattes, H. Muirhead, G. Occhialini and C. F. Powell (LATTES C. M. G. ; MUIRHEAD,) in 1947, kaons, gluons, W and Z bosons, quarks and more recently in 2012 the Higgs boson with the ATLAS and CMS experiments at CERN.

After the discovery of pions, a new formulation of the classification of particles become necessary, and the first description was made by Sakata in the "On a Composite Model for New Particles"(SAKATA, 1956), amplified by "A Unified Model for Elementary Particles"by Maki, Nakagawa, Ohnuki and Sakata in 1960 (MAKI M. NAKAGAWA; SAKATA., 1960) and 1962 (MAKI; SAKATA., 1962) and turned more complete with the inclusion of quarks by Gell-Mann and Zweig (GELL-MANN, ; ZWEIG, 1964) in 1964. All those works together form The Standard Model of particle physics, which describe the fundamental forces: eletromagnetic, weak and strong interactions and the classifications of all those elementary particles.

The RHIC includes knowledge from the elementary particle physics, in the collision process, and also a interlude with large scale facing to the search of matter in the early universe called Quark-Gluon plasma (QGP). The QGP is a state of matter which only exist in a rare extreme conditions of density and high temperature. It only exist for a really short period and was found in experiments on the Large Hadron Collider (LHC) at CERN (RAFELSKI,) in 2000.

The path to discover the QGP, and obtain the observables, flow harmonics and jet quenching, in the relativistic heavy ion collisions is long and involves a range of process. Those process can be roughly divided in three main stages: pre-thermalization, collision evolution, and decoupling. In the principle we have two beams of some species such as gold, uranium, lead, electron-electron, proton-proton etc. The collider accelerate those beams in velocity near of light speed c and with a specific mechanism is possible to make a tiny beam well located spatially.

Following the trajectory of the beam, in some point of time and space the beams collide, and start the collision process. If we think in the common way, a good approach to know the constituents of some matter is for example colliding it on some barrier and see its parts breaking down. In RHIC the same occurs, but in this case we are interested in the constituents of the beams, or to be more specific, in the constituents of the particle.

There is many models to describe the collision process. A geometric description of this process is made by Glauber Monte-Carlo model (MILLER M. L.; REYGERS; SANDERS STEPHEN, 2007). In this model we consider that when the nuclei collide those collisions is analysed as a series of binary collisions, i.e., a sequence of proton-proton collisions. We consider one beam as a target and other one as a projectile, and define a tube flux. For each tube flux we have some essential relations to be derived as the probability of interaction of nucleons and the differential cross-section σ.

The differential cross-section σ is one of the most relevant informations about the system, once it show us the area that measures the probability of collisions between target and projectile. Following this, we also recall for the impact parameter b, which measure the distance between the center of each nuclei, and the number of participants N, once we is well-know that not all nucleons interact, and the quantity which tell us about the effective participants is N.

We also know that nuclei are made by nucleons, protons and neutrons, on the other hand nucleons are made of quarks. The quarks are maintained together in the nucleons by the strong force. That information will be extremely relevant when we present the decoupling stage and study their details.

We can consider the collision stage also in the Quantum Field Theory (QFT) approach. In QFT, the $e^+e^- \rightarrow \mu^+\mu^-$ process is the most elementary process governed by quantum electrodynamics (QED). Strong interactions, on the other hand, are described by non-Abelian gauge theory, known as quantum chromodynamics (QCD).

More sophisticated theory might be able to evaluate hard processes such as quark+proton, even p-p collisions. In the context of perturbative theories, to obtain the differential cross-section σ for the above processes, we use the Feynmann rules.

In principle, for RHIC, one can not straightforwardly employ the Feynman rules to obtain σ for soft process owing to the highly non-perturbative nature of the latter. However, as an educated estimation, the Glauber Monte-Carlo approach views the process as superpositions of p-p collisions evaluated by QCD, among other means. To reconstruct a relation for σ, one makes use of the concept of flux tube together with the probability of interaction between nucleons. In this framework, we also may estimate the number of participants in each collision.

Independently of the theory used in the collision process, the next stage is concerning to the collision evolution. A short time after the collision process, the thermalization occurs and the system goes to a hottest temperatures. From this point, we need to use a theory to describe the evolution of the system, this theory is the relativistic hydrodynamics.

The relativistic hydrodynamics study a continuum medium, the collision evolution in this case, in the covariant framework. The hydrodynamics recall to the charge and energy-momentum conservation together with the second law of thermodynamics. The equations of motion, the energy-flux tensor and transport coefficients as viscosities are described and needed to be well defined and solved in this frame regarding information of the system.

Usually we can start from the ideal fluids model, which have six equations with six unknowns variables. For a more realistic model, we can add bulk and/or shear viscosity, η, and ζ respectively.

The price to be paid to add viscosity is the increasing of the number of equations to be solved. The theories which include bulk and shear are called as first and second order theories.

Landau and Lifshitz proposed a theory (LANDAU L. D., 1958) based on the covariant version of Navier-Stokes equation of classical hydrodynamics. Although this approach shows some aspects of dissipative hydrodynamics, the theory leads to causality violation. Looking into a new approach free of this causality violation, Muller (MULLER, 1967), Israel, and Stewart (ISRAEL, 1979) developed a new theory.

This theory is called as second-order theory and its include bulk and shear viscosity and remove the causality violation. One crucial point of viscous relativistic hydrodynamics is that the theory has good acceptance with the experimental data from STAR and Phobos collaborations.

The system keep evolving until the particles cross the freeze-out hyper-surface. These hyper-surface is characterized by a freeze-out temperature, originally proposed by the Cooper-Frye prescription (COOPER F. ; FRYE,). Once this temperature is achieved, the decoupling stage starts. We comment earlier about the nucleon constituents, and in the decoupling state, the hadrons which made the nuclei decoupling and become non-interacting objects allowed to traveling freely in the space.

The decoupling occurs instantly when the particles cross the hyper-surface, generating free particles and other observables which can be measured in the detectors. Those observables are the most important quantities in the RHIC. Examples of observables are the transverse momentum p_t, transverse mass m_t, the rapidity and pseudo rapidity distribution and the flow harmonics v_i.

Specially flow harmonics have a more important place in this shelf, once it represents how the energy is distributed. v_1 is know as direct flow, v_2 is know as elliptic flow and its indicates the asymmetry of energy flow in space, v_3 is the triangular flow, and others are simply v_4, v_5, and v_6. All those flow are defined by a simple relation, using the reaction plane. The relation and the reaction plane will be described posteriorly.

Some recent studies in the past decade suggested that the geometric form of the nuclei in relativistic collisions can affect the observables (ADAMCZYK, ; GIACALONE,), especially the elliptic flow. With this motivation we proposed to verify how the observables can be changed if we introduce a geometric deformation of nuclei. We are engaged to use two different types of nuclei, Au and U. For Au nuclei we will analyze the change in the observables for non deformed and deformed nuclei, while for U nuclei we will perform an analysis with a non deformed nuclei and two different types of deformed nuclei.

We will perform a numerical study of relativistic heavy-ion collisions based on hydrodynamical models. With this in mind, we will use the Complete Hydrodynamical Evolution SyStem, or simply CHESS code, developed to reproduce all stages of RHIC. The code is a set of three well-known codes largely used in RHIC: the Reduced Thickness Event-by-event Nuclear Topology ((TrENTo) (MORELAND J. C.; BERNHARD,) for the collision stage, Viscous Hydro Evolution (vHLLE) (HUOVINEN P.; BLEICHER,) for the time-space evolution, and the THERMal heavy IoN generATOR version 2 (THERMINATOR 2) (CHOJNACKI M. LAJ; KISIEL, 2002) which carry informations about the decoupling stage.

We will divide this study as follow: After this brief introduction, we will present in the chapter

2 all theory envolved in the three stages of RHIC, describing the Glauber Model for collision, the Hydrodynamics and the Cooper-Frey prescription for decoupling of hadrons. The last subsection of chapter 2 is devoted to the equation of state. In chapter 3 we will describe the observales, the quantities which carry relevant physical information and be detected in the detectors.

Chapter 3 will be used to present the numerical codes TrENTo, vHLLE, THERMINATOR 2 and the CHESS code. In Chapter 5 we will present the partial results obtained so far by CHESS code and the future works.

2 THEORETICAL BACKGROUND

In this chapter we will discuss all theoretical basis envolved in the RHIC. We will start from the first stage of RHIC, the collision stage. As we discussed earlier, after the establish of the standard model of particles we know that the nuclei are composed by nucleons, i.e, protons, neutrons, and consequently by quarks. We also know that the description of collisions can be described by classical mechanics or in quantum mechanics, related to scattering problems.

Even with a good description in these cases, those approaches can't be applied directly to a many-body system as we have in RHIC. To treat the many-body systems, the Glauber model emerged. It's important to write that the Glauber model is not the unique model to describe the collision process, or initial conditions in RHIC, there are modern, as well as intrinsically non-perturbative approaches that describe the collisions such as IP-Glasma Model (B. SHEN C.,) based on the concept of gluon condensation and AdS/CFT correspondence (RAMALLO,) based on the holographic principle. The Glaubel Model is the subject of the second section of this chapter.

In section 2.3 we will show the system spacetime evolution. In this part will use the hydrodynamics, a well-known and remarkable theory which had it success proved with the discovery of the QGP. Hydrodynamics solve equations of motion, charge current and energy-momentum conservation describing the behavior of matter generated in the collision. Equations of states are described in order to help us to describe the phase transition between the QGP and HG.

Section 2.4 is devoted to a discussion about the decoupling of the system. In this part we will describe the Cooper-Frye prescription, an elegant way do describe the particle distributions and the final observables.

The last section is used to describe the observables, the quantities which we can measure directly or indirectly in the detector. Those quantities such as particle distributions and elliptic flow are fundamental due to its physical content.

2.1 COLLISION

The scattering process is well know in physics since Newton's experiment with prisms, and latter with Rutherford experiments with gold foil which led him to Rutherford model of atom. Whit the development of Quantum Mechanics, the scattering theory also be applied to quantum phenomena. All those experiments are simpler to be treated in the mathematical context.

In RHIC, until 1958 there is no calculations to treat the scaterring of many-body nuclear systems. The Glauber theory proposed a firm basis, and a consistent description of experimental data for projectile, and target systems collisions (MILLER M. L.; REYGERS; SANDERS STEPHEN, 2007). Firstly applied to a proton-deuterium collisions, latelly amplified to nuclei-nuclei collisions, the Glauber model is one of the most used models to describe RHIC initial stage.

2.1.1 Glauber Monte-Carlo Model

The Glauber model is based on nuclear geometry, treating the nucleus-nucleus collision as a series of nucleon-nucleon collisions, also named binary collisions, which is the essential key ingredient of the model. The Glauber model proposition has the following hypothesis:

A) Nuclei-nuclei collisions can be considered as a series of binary collisions: First how the beam generated by particle accelerator is tiny, we can consider with a good approximation that the beam has a unique nuclei. We set one nuclei to be the target and the other one to be the projectile. Both have the same speed, near of c, with opposite direction. Those nuclei are intact before the collision and has a large number of nucleons, but not all nucleons will interact in the collision process.

There is a overlap region in the space where the nucleons interact, while other remain intact. Nucleons in the overlap region are called usually as participants, and the others are called spectators. In the collision process thousand of particles are produced. Even seems that it is intractable, in the Glauber model we assume that once we know how to treat a proton-proton collision, we can consider all collisions as a series of proton-proton collisions.

B) Nuclei-nuclei collisions obey a linear trajectory:

C) All nuclei are considered as a three-dimensional body with the density given by Woods-Saxon perfil: The Woods-Saxon perfil for non-deformed, or symmetric nuclei, is given by the following formula:

$$\rho_{A,B}^{part}(x,y,z) = \frac{\rho_0}{1+\exp\left[\frac{(r-R_{A,B})}{a}\right]}, \tag{1}$$

where A and B denote each nucleon, ρ is the initial density, $r = \sqrt{x^2+y+z^2}$, a is the diffusion parameter, and $R_{A,B}$ is the radius of nucleon.

For the deformed nuclei the Woods-Saxon perfil is given by:

$$\rho_{A,B}^{part}(x,y,z) = \frac{\rho_0}{1+\exp\left[\frac{(r-R_{A,B})(1+\beta_2 Y_{20}+\beta_4 Y_{40})}{a}\right]}, \tag{2}$$

where β_2 and β_4 are deformation factors, Y_{20} and Y_{40} are the spherical harmonics. All those parameters described below has a special values and are related to the type of nuclei and will be discussed more carefully in the numerical implementation by TRENTO.

D) The nuclei can be deformed:

E)The collisions only occurs if the distance between the nucleons reach the minimum distance given by the relation $\sqrt{\frac{\sigma_{NN}}{\pi}}$:

With those few assumptions in mind, we can start to describe the Glauber model considering the figure Figura 1. Two nuclei A, and B, named target and projectile respectively have opposite directions assuming the collision will occurs in z-direction. We define the impact parameter b as a quantity to define the distance between each nuclei center, s will be the distance between some element in the nuclei in relation to its center.

From figure Figura 1 it's clear to see that there is an overlap area between target and projectile. We show in figure Figura 2 the beam view which clarifies it:

Figura 1 – Side view

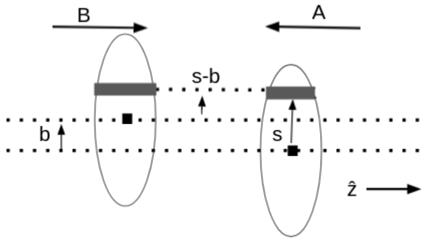

Font: Author's production.

Figura 2 – Beam view

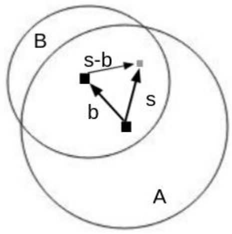

Font: Author's production.

We will describe the next relations in this overlap area. Using the Woods-Saxon perfil (2) or (2), one can define the probability of interaction as:

$$\hat{T}_A(s) = \int_{-\infty}^{+\infty} \rho_A(s,z)dz. \tag{3}$$

Once we define the nuclear thickness, we can define the thickness function as:

$$\hat{T}_{AB}(b) = \int_{-\infty} \hat{T}_A(s)\,\hat{T}_B(s-b)\,d^2s. \tag{4}$$

The thickness functions is interpreted as the effective overlap area for which a target can interact with the projectile.

The probability of an interaction occurs is given by the distribution:

$$P(n,b) = \binom{AB}{n}\left[\hat{T}_{AB}(b)\sigma_{inel}^{NN}\right]^n\left[1-\hat{T}_{AB}(b)\sigma_{inel}^{NN}\right]^{AB-n}, \tag{5}$$

where the σ_{inel}^{NN} is the nucleon-nucleon inelastic cross section.

The total probability of an interaction between the nuclei A and B is given:

$$\frac{d^2\sigma_{inel}^{A+B}}{db^2} = 1-\left[1-\hat{T}_{AB}(b)\sigma_{inel}^{NN}\right]^{AB}, \tag{6}$$

and assuming b can be replaced by the scalar distance the total cross section is:

$$\sigma_{inel}^{A+B} = \int_0^{\infty} 2\,\pi\,db\left(1-\left[1-\hat{T}_{AB}(b)\sigma_{inel}^{NN}\right]^{AB}\right), \tag{7}$$

The total number of nucleon-nucleon collisions:

$$N_{coll}(b) = AB\hat{T}_{AB}(b)\sigma_{inel}^{NN}. \tag{8}$$

The total number of participants N_{part} is obtained by:

$$\begin{aligned} N_{part}(b) = A\int \hat{T}_A(s)(1-[1-\hat{T}_B(s-b)\sigma_{inel}^{NN}])^B d^2s+ \\ B\int \hat{T}_B(s-b)(1-[1-\hat{T}_A(s)\sigma_{inel}^{NN}])^A d^2s. \end{aligned} \tag{9}$$

2.2 INITIAL CONDITIONS

The initial conditions (IC) are a set of quantities used in RHIC to modulate the entire system. After a some given time τ after the collision, the system arises its thermal equilibrium. One can find some different values of τ parameter in the literature (), we will use the value $\tau_0 = 0.6fm$.

There is two types of initial conditions, the **smooth initial conditions** or **event-by-event** initial conditions. In the smooth initial condition we have a statistic average of initial hydrodynamics quantities over events. We compute the hydrodynamics once and obtain the observables. In the event-by-event initial conditions, we compute the hydrodynamics for each event and after all those events we will compute an average over its events to compute the final observables.

2.2.1 Eccentricity

Another quantity which constitute the set of initial conditions is the eccentricity. The eccentricity measures the spatial anisotropy of the system. According to Bhalerao (BHALERAOA RAJEEV S. OLLITRAUL, 2006) we define the eccentricity as

$$\epsilon = \frac{< y^2 - x^2 >}{< y^2 + x^2 >}, \tag{10}$$

where the pair (x, y) refers to the participant nucleon position and the $<>$ indicates an average over participant nucleons.

Due to event-by-event fluctuations in the participant nucleon we also can define the participant eccentricity as follow:

$$\epsilon_{part} = \frac{\sqrt{(\sigma_y^2 - \sigma_x^2)^2 + 4(\sigma_{xy})^2}}{\sigma_y^2 + \sigma_x^2}, \tag{11}$$

with σ_x^2, σ_y^2, and σ_{xy} defined as follow:

$$\sigma_x^2 =< x^2 > - < x >^2$$

$$\sigma_y^2 =< y^2 > - < y >^2$$

$$\sigma_{xy}^2 =< xy > - < x >< y >$$

.

For high order Fourier coefficient, Teaney and Yan (TEANEY; YAN,) introduce an expansion relating eccentricity and the orientation in each event as:

$$\epsilon_{n,n}e^{in\Phi_{n.n}} = \epsilon_{n,n}e^{in\Phi_{n.n}} = -\frac{< r^n\, e^{i\,n\,\phi} >}{< r^n >}, \tag{12}$$

with r being the position and ϕ the angle in the transverse plane.

2.3 COLLISION EVOLUTION - HYDRODYNAMICAL MODEL

After the initial stage has been complete, the matter goes to the space-time evolution. At this point equations of motion, as in classical mechanics, needed to be solved. In this context emerged the relativistic hydrodynamics, a sophisticate theory capable to describe the system evolution in space-time with the inclusion of viscosity.

The Hydrodynamical model describe the space-time evolution in the relativistic heavy ion collisions. We show in figure Figura 3 the entire system evolution.

Figura 3 – System evolution

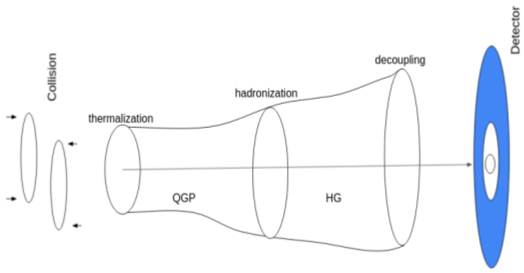

Font: Author’s production.

After the collision a hot fireball is created and a new type of matter emerges, the quark-gluon plasma. Actually this new type is a primordial matter found in the earlier time of Universe under extreme conditions with high temperature and density. After some time the matter becomes cold and can be described by equations of motion given by hydrodynamics model. In some point with given (T, μ_b), temperature and barionic density, occurs the phase transition between the QGP and the hadron gas or hadronic phase (HG). After the phase transition and when the system arise the freeze-out temperature the hadrons decoupling and can travel freely and be detected by the detector.

The topic of this section is the hydrodynamics. The hydrodynamics model is used to describe the motion of fluids on their local property (SOUZA R. D. KOIDE,). The success of this model as a tool of the phenomenological context in the description in RHIC and LHC. After the discovery of QGP and the signatures of collective behavior the relativistic hydrodynamics had its success proved (FLORKOWSKI W. HELLER,).

The heart of hydrodynamics is the conservation equations. In this theory we must solve the conservation of energy-momentum tensor $(T^{\mu\ \nu})$ and charge current j_i^{ν} given by:

$$\partial_{\nu} T^{\mu\nu} = 0, \tag{13}$$

$$\partial_\nu\, J_i^\mu = 0, \tag{14}$$

for i be each conserved charges.

From the energy-momentum conservation we have a set of 4 equations, and for current charge conservation N equations. So we need to solve 4+N equations but a brief analysis show that due to symmetry of $(T^{\mu\ \nu})$, a 2-rank tensor, and the charge current a four-vector, we have a 10+4N variables, therefore we cannot perform a direct computation.

In order to rearrange it, we will introduce the Milne coordinates, or hyperbolic coordinates. In this coordinate system we define the variables τ and η as follow:

$$\begin{aligned} \tau &= \sqrt{t^2 - z^2} \\ \eta &= \frac{1}{2}\ln\big(\frac{t+z}{t-z}\big) \end{aligned} \tag{15}$$

the inversion yields:

$$\begin{aligned} t &= \tau\ \cosh\eta \\ z &= \tau\ \sinh\eta. \end{aligned} \tag{16}$$

The Minkowski spacetime metric in this coordinate system will be:

$$g_{\mu\,\nu} = \begin{bmatrix} 1 & 0 & 0 & 0 \\ 0 & -1 & 0 & 0 \\ 0 & 0 & -1 & 0 \\ 0 & 0 & 0 & -\tau^2 \end{bmatrix}. \tag{17}$$

We know the covariant derivative for a 2-rank tensor and four-vector is:

$$\partial_\nu A^{\mu\nu} = \partial_\alpha A^{\mu\nu} + \Gamma^\mu_{\alpha\beta}\, A^{\nu\beta} + \Gamma^\nu_{\alpha\beta}\, A^{\mu\beta}, \tag{18}$$

$$\partial_\nu A^\mu = \partial_\nu A^\mu + \Gamma^\nu_{\mu\beta}\, A^{\mu\beta}, \tag{19}$$

with

$$\Gamma^\nu_{\mu\beta} = \frac{1}{2} g^{\alpha\beta}(\partial_\mu g_{\beta\nu} + \partial_\nu g_{\beta\mu} - \partial_\beta g_{\mu\nu}),$$

being the Christoffel symbols.

We first must compute all non-vanishing Christoffel symbols. Direct computation show that:

$$\Gamma^\tau_{\eta\eta} = \tau, \quad \Gamma^\eta_{\eta\tau} = \Gamma^\eta_{\tau\eta} = \frac{1}{\tau} \tag{20}$$

Once we have the Christoffel symbols we can compute the equation of each component.

Therefore we summarize in the following form:

$$\begin{aligned} \partial_\nu T^{\tau\nu} + \tau T^{\eta\eta} + \frac{1}{\tau}T^{\tau\tau} \\ \partial_\nu T^{x\nu} + \frac{1}{\tau}T^{x\tau} \\ \partial_\nu T^{y\nu} + \frac{1}{\tau}T^{y\tau} \\ \partial_\nu T^{\eta\nu} + \frac{3}{\tau}T^{\eta\tau} \\ \partial_\nu j_i^{\mu} + \frac{1}{\tau}j_i^{\tau} \end{aligned} \tag{21}$$

The set of equations given in equation (21) is the set of equations of motion to be solve in hydrodynamics. Now, we need a proper description for $T^{\mu\nu}$ and j_i^{ν}.

In the next subsections we are going to describe the ideal hydrodynamics, also known as non-dissipative hydrodynamics, and dissipative hydrodynamics including some important mathematical tools used to describe it.

2.3.1 Ideal Hydrodynamics

The first assumption that we will show in hydrodynamics is the ideal hydrodynamics. In this regime we assume a null viscosity and energy-momentum tensor is the same used in general relativity for a perfect fluid assuming the following form:

$$T^{\mu\,\nu} = \begin{bmatrix} \epsilon & 0 & 0 & 0 \\ 0 & P & 0 & 0 \\ 0 & 0 & P & 0 \\ 0 & 0 & 0 & P \end{bmatrix}, \tag{22}$$

and the current:

$$J_i^{\mu} = \begin{bmatrix} n_i \\ 0 \\ 0 \\ 0 \end{bmatrix}. \tag{23}$$

Using those relations one can construct the energy-momentum tensor and the four-charge current for the ideal or non-dissipative hydrodynamics as:

$$T_{id}^{\mu\nu} = \Lambda_{\alpha}^{\mu}\Lambda_{\beta}^{\nu}T^{\alpha\beta} \tag{24}$$

$$j_{i\;id}^{\nu} = \Lambda_{\alpha}^{\nu}J_i^{\alpha}, \tag{25}$$

which lead us to the following expressions:

$$T_{id}^{\mu\nu} = \epsilon u^{\mu}u^{\nu} - P\Delta^{\mu\nu} \tag{26}$$

$$j_{i\ id}^{\nu} = n_i u^{\nu}. \tag{27}$$

We identify $\Delta^{\mu\nu}$ as the orthogonal projector to the four-velocity of the fluid, it has the properties:

$$\Delta^{\mu\nu} u_{\mu} = \Delta^{\mu\nu} u_{\nu} \tag{28}$$

$$\Delta^{\mu\nu} \Delta_{\nu}^{\alpha} = \Delta^{\mu\alpha}. \tag{29}$$

One of the most important facts in the ideal hydrodynamics is that the entropy is conserved. The equation for entropy conservation is:

$$\partial_{\nu} S^{\nu} = \partial_{\nu}(s u^{\nu}) = 0, \tag{30}$$

where $S^{\nu} = su^{\nu}$is the four-entropy current.

2.3.2 Dissipative Hydrodynamics

For a more realistic description, we need to add the viscosity. This need is not only for an aim to describe better the system itself, but due to the fact that in hight p_T regime the collective flow can't be reproduced using the ideal hydrodynamics, the viscosity will play an important role in order to reduce the pressure and decrease the harmonics (MURONGA,).

The energy-momentum tensor and the charge current is described as:

$$T^{\mu\nu} = T_{id}^{\mu\nu} + \delta\, T^{\mu\nu} \tag{31}$$

$$j_i^{\nu} = j_{i\ id}^{\nu} + \delta\, j_i^{\nu}, \tag{32}$$

where the label id is related to the ideal contribution, and δ is related to the viscous contribution.

We can explicitly show the viscous contribution through the relations:

$$\delta\, T^{\mu\nu} = \pi^{\mu\nu} + \Delta^{\mu\nu}\Pi, \tag{33}$$

$$\delta\, j_i^{\nu} = V^{\nu}, \tag{34}$$

with π, Π, and V^{ν} being the shear and bulk viscosity, and the charge diffusion.

Finally, using the viscous correction (33), and (34) into equations (31), and (36) together with the energy-momentum tensor, and charge current related to the ideal hydro and we have:

$$T^{\mu\nu} = \epsilon u^{\mu} u^{\nu} - (P + \Pi)\, \Delta^{\mu\nu} + \pi^{\mu\nu} \tag{35}$$

$$j_i^\nu = n_i u^\nu + V_i^\nu. \tag{36}$$

In equations (35) and (36) the terms $\Pi, \pi^{\mu\nu}$ and V_i^ν are identified as volumetric viscosity, shear viscosity tensor and the charge diffusion current. We assume there is no vorticity, it means that $V_i^\nu = 0$, due to null barionic density. One can easily see under this new description, the $T^{\mu\nu}$ become non-diagonal.

The main questions now is: how to obtain the relations for Π, and $\pi^{\mu\nu}$?. The so-called First Order theory is based on the covariant formulation of Classical Navier-Stokes hydrodynamics, and there is some freedom according to the author. For example, according to Landau (**??**), which choose the rest frame in which the energy flux is null we can obtain the following relation:

$$u_\nu \, T^{\mu\nu} = \epsilon \, u^\mu, \tag{37}$$

by multiplying both sides of equation (26) by u_ν, and setting $u_\nu \, \pi^{\mu\nu} = 0$. How the conservation of energy-momentum tensor should be preserved we must do:

$$u_\mu \, \partial_\nu \, T^{\mu\nu} = 0. \tag{38}$$

Deriving the energy-momentor tensor (35), with some math and using the second law of thermodynamics we can write the volumetric viscosity, and the shear viscosity in the Navier-Stokes formalism as follow:

$$\pi_{NS}^{\mu\nu} = \eta_v \left(\Delta^{\mu\lambda} \, \partial_\lambda u^\nu + \Delta^{\nu\lambda} \, \partial_\lambda u^\mu\right) - \frac{2}{3} \, \eta_v \, \Delta^{\mu\nu} \, \partial_\lambda \, u^\lambda \tag{39}$$

$$\Pi_{NS} = -\zeta_v \partial_\lambda \, u^\lambda. \tag{40}$$

However, this choice lead us to a no causal propagation, $v > c$ and it cannot be applied according to Hiscock and Lindblom (HISCOCK,). In order to solve this instability and causal propagation, Israel and Stewart (ISRAEL, 1979) in 1970's proposed a new theory, called second-order theory. In this formalism we have the volumetric viscosity, and the shear viscosity tensor is given by:

$$\pi^{\alpha\beta} = \pi_{NS}^{\alpha\beta} - \tau_\pi u^\nu \partial_\nu \pi^{\alpha\beta} - \frac{T}{2} \pi^{\alpha\beta} \partial_\nu \Big(\frac{u^\nu}{T} \tau_\pi\Big) \tag{41}$$

$$\Pi = \Pi_{NS} - \tau_\Pi u^\nu \partial \nu \Pi - \frac{T}{2} \Pi \partial_v \Big(\frac{u^\nu}{T} \tau_\Pi\Big), \tag{42}$$

where τ_π and τ_Π are the relaxation time for volumetric and shear viscosity. Equations (41), and (42) are called Israel-Stewart equations.

2.4 DECOUPLING

The final stage that we should describe in RHIC theory is the decoupling. We said earlier that the hadrons decoupling after reach some temperature. This temperature is called the freeze-out temperature, denoted by T_{fo}. In fact we assume there is a hypersurface, usually denoted by the letter Σ, which has a constant temperature, the freeze-out temperature.

This assumption become an important way to describe the decoupling of hadrons after Cooper-Frye (COOPER, ; COOPER; SCHONBERG.,) exposed the following main ideas:

i) The hypersurface has an infinitesimal thickness;

ii) Once the particles pass through the hypersurface reaching freeze-out temperature the particles decoupling instantly;

iii) After the decoupling the particles won't interact and they can freely travel.

This model is known as Cooper-Frye prescription and become an important tool nowadays.

We assume that the number of particles passing through an infinitesimal hypersurface element $d\Sigma$ is:

$$N = \int_{\Sigma} d\Sigma_{\mu}\, j^{\mu}, \tag{43}$$

where j^{μ} is the four-current given by

$$j^{\mu} = \int \frac{d^3p}{E}\, p^{\mu}\, f(x,p), \tag{44}$$

for p^{μ}, and $f(x,p)$ being the four-momentum and the distribution function.

Substituting equation (44) in equation (43) we have the total number of particles as:

$$N = \int \int_{\Sigma} d\Sigma_{\mu}\, \frac{d^3p}{E}\, p^{\mu}\, f(x,p). \tag{45}$$

We can rewrite (46) in order to obtain the Cooper-Frye equation:

$$E\,\frac{d^3N}{d^3\vec{p}} = \int_{\Sigma} d\Sigma_{\mu}\, \frac{d^3p}{E}\, p^{\mu}\, f(x,p), \tag{46}$$

which show to us the total number of of particles which will be detected in the detectors.

To complete the description we must provide a hypersurface parametrization, as well a description of the elements inside of the integral, i.e, the four-momentum p^{μ}, the distribution function $f(x,p)$, and also the volume element $d\Sigma$.

We can give two paths to its description, through a 2+1D surface which has some symmetries, or 3+1D surface without symmetry. Those arguments will be presented in the section 4.2 as well a complete description of the elements above. In next section we will describe the equation of state, an important way to describe the physical content during the space-time evolution.

2.5 EQUATION OF STATE (EOS)

The equations of State (EoS) are used to describe matter, like fluids, solids and gases. Those equations relates quantities related to matter such as temperature, pressure, density, etc. In this section we are going to describe two equations of states (EoS) which will be used in the future.

We know that the matter created in RHIC is the quark gluon plasma (QGP) during the collision process. After the thermalization and evolution described by the hydrodynamics occurs the process of decoupling, and then the matter changes to the hadron gas (HG), or to be more specifically, occurs a phase transition.

In this section we are going to describe the first Order equation of state (FO-EoS). The FO-EoS has a phase which contains simultaneosly the QGP and HG in the phase transition. We will describe first the QGP, after the HG and the last topic of this section is devoted to a brief explanation in the first order EoS.

2.5.1 Quark-Gluon Plasma

We will describe the equations os state for the QGP. We start the deduction for the pressure P, considering that in the the phase space we have the number of quarks with momentum p in the interval dp is given in according to the Fermi-Dirac distribution:

$$dN_q = \frac{g_q \, 4\,\pi\, p^2\, V\, dp}{(2\,\pi)^3} \Big[\frac{1}{e^{(p-\mu_q)/T}+1}\Big], \tag{47}$$

where $g_q = N_c\, N_s\, N_f$ is the degeneracy of quarks, μ_q the chemical potential.

For the antiquarks we have:

$$n_{\bar{q}} = \frac{g_q}{(2\,\pi)^3} \int 4\,\pi\, p_0^2\, dp_0 \Big[\frac{1}{e^{(p+\mu_q)/T}+1}\Big]. \tag{48}$$

The number of quarks and antiquarks are equal, and the potencial $\mu_q = 0$. Plugging $\mu_q = 0$ into the last equation we have:

$$E_q = \frac{g_q\, 4\pi\, V}{(2\,\pi)^3} \int_0^\infty \frac{p^3\, dp}{1+e^{p/T}}, \tag{49}$$

using $z = p/T \implies p = z\, T$, so $dp = T\, dz$, therefore we have:

$$E_q = \frac{g_q\, V}{2\,\pi^2} \int_0^\infty \frac{z^3\, T^3\, T dz}{1+e^z}, \tag{50}$$

which implies in:

$$E_q = \frac{g_q\, V T^4}{2\,\pi^2} \int_0^\infty \frac{z^3\, dz}{1+e^z}. \tag{51}$$

Using the expansion of $[1+e^{-x}]^{-1} = [1+e^{-x}+e^{-2x}+ ... = \sum_{n=0}^{\infty} e^{nx}$ we can rewrite equation (51) as:

$$E_q = \frac{g_q\, V T^4}{2\,\pi^2} \int_0^\infty z^3\, e^{-z} dz \sum (-1)^n\, e^{-nz}. \tag{52}$$

The gamma function Γ is given by:

$$\Gamma(z) = \int_0^\infty t^{z-1} e^{-t} dt,$$

we easily identify in equation (52) the $\Gamma(4)$, therefore:

$$E_q = \frac{g_q VT^4}{2\,\pi^2}\,\Gamma(4)\,\sum (-1)^n\,\frac{1}{(n+1)^4}. \tag{53}$$

Observe that the term in the summation can be rewrite using the odd and pair terms:

$$\sum_n (-1)^n\,\frac{1}{(n+1)^4} = \sum_{m=1,3,5,\ldots} \frac{1}{m^4} - \sum_{m=2,4,6,\ldots} \frac{1}{m^4} = \sum_{m=1,3,5,\ldots} \frac{1}{m^4} - 2 \sum_{m=2,4,6,\ldots} \frac{1}{(2m)^4}, \tag{54}$$

from the Riemann zeta function $\zeta(x) = 1/m^x$, we are able to write:

$$\sum_n (-1)^n\,\frac{1}{(n+1)^4} = (1 - 2^3)\zeta(4), \tag{55}$$

and therefore:

$$E_q = \frac{g_q VT^4}{2\,\pi^2}\,\Gamma(4)\,(1 - 2^3)\zeta(4). \tag{56}$$

Using the fact that $\Gamma(4) = 6$, and $\zeta(4) = \frac{\pi^4}{90}$ we get:

$$E_q = \frac{g_q VT^4}{2\,\pi^2}\,6\,(1 - 2^3)\,\frac{\pi^4}{90} \implies E_q = \frac{7}{8}\,g_q\,V\,T^4\,\frac{\pi^2}{30}. \tag{57}$$

The equation (57) is the energy of the system due to quarks. We can easily obtain the energy density of quarks from equation (57):

$$\epsilon_q = \frac{7}{8}\,g_q\,T^4\,\frac{\pi^2}{30}. \tag{58}$$

We also can evaluate the pressure P using the fact that $P = \frac{1}{3}E/V$, we have:

$$P_q = \frac{7}{8}\,g_q\,T^4\,\frac{\pi^2}{90}. \tag{59}$$

The same procedure can be done in order to have the energy, density energy and pressure for anti-quarks, the equations are the following:

$$\epsilon_{\bar{q}} = \frac{7}{8}\,g_{\bar{q}}\,T^4\,\frac{\pi^2}{30} \tag{60}$$

$$P_{\bar{q}} = \frac{7}{8}\,g_{\bar{q}}\,T^4\,\frac{\pi^2}{90}. \tag{61}$$

Summing expressions (58) and (60) we have the total energy density of a gas of quarks and antiquarks:

$$\epsilon_{q\bar{q}} = \frac{7}{8}\,(g_q + g_{\bar{q}})\,T^4\,\frac{\pi^2}{30}. \tag{62}$$

The total pressure will be given by the sum of equations (59) and (61):

$$P_{q\bar{q}} = \frac{7}{8}\,(g_q + g_{\bar{q}})\,T^4\,\frac{\pi^2}{90}. \tag{63}$$

Once we write the equations for quark and antiquark, we can write the same equations for gluons. Assuming a null potential μ_g and the Bose-Einstein distribution we have the energy given by:

$$E_g = \frac{g_g\,V}{2\,\pi^2}\int_0^\infty \frac{p^3\,dp}{e^{p/T}-1}, \tag{64}$$

with g_g being the degeneracy factor for gluons.

We will follow the same procedure we did before, taking $p = z\,T \implies dp = T\,dz$, then:

$$E_g = \frac{g_g\,V}{2\,\pi^2}\int_0^\infty \frac{(z\,T)^3\,T\,dz}{e^z - 1} = \frac{g_g\,V}{2\,\pi^2}\int_0^\infty z^3 e^{-z} dz \sum_n e^{-nz}, \tag{65}$$

but $\sum_n e^{-nz} = \sum \frac{1}{(n+1)^4} = \zeta(4)$, and $\int_0^\infty z^3\,e^{-z}dz = \Gamma(4)$, also using $\Gamma(4) = 6$, and $\zeta(4) = \frac{\pi^4}{90}$ we have:

$$E_g = g_g\,V\,T^4\,\frac{\pi^2}{30}. \tag{66}$$

The gluons energy density and pressure will be:

$$\epsilon_g = g_g\,T^4\,\frac{\pi^2}{30}, \tag{67}$$

and

$$P_g = g_g\,T^4\,\frac{\pi^2}{90}. \tag{68}$$

Once we have expressions for quarks and gluons we can write the density energy ϵ, and pressure P for the gas of quarks and gluons summing equations (62), (67) and (59) and (68) respectively:

$$\epsilon_{QGP} = \left[g_g + \frac{7}{8}(g_q + g_{\bar{q}})\right]\frac{\pi^2}{30}T^4 \tag{69}$$

$$P(T)_{QGP} = \left[g_g + \frac{7}{8}(g_q + g_{\bar{q}})\right]\frac{\pi^2}{90}T^4. \tag{70}$$

The relations (69) and (73) are valid in the high-temperature regime. For low temperature the interaction between quarks and gluons should be considered. The MIT bag model is used tho describe this interaction (CHODOS R. L. JAFFE,). In this model we add a constant $\mathbf{B}$ called bag constant in the equations (69), and (73) as follow:

$$\epsilon_{QGP} = \left[g_g + \frac{7}{8}(g_q + g_{\bar{q}})\right]\frac{\pi^2}{30}T^4 + \mathbf{B} \tag{71}$$

$$P(T)_{QGP} = \Big[g_g + \frac{7}{8}(g_q + g_{\bar{q}})\Big]\frac{\pi^2}{90}T^4 - \mathbf{B}. \tag{72}$$

We can obtain the entropy using the relation $s = (\epsilon + P)/T$, and equations (71) and (71):

$$s_{QGP} = 4\Big[g_g + \frac{7}{8}(g_q + g_{\bar{q}})\Big]\frac{\pi^2}{90}T^3. \tag{73}$$

In next topic we will describe the hadronic phase.

2.5.2 Hadron gas

The strong interaction of hadrons is not easy to be used in the EoS, howhever for the hadron gas phase we can start the construction the EoS using the grand canonical esemble for an ideal gas of quantum particles. In this ensemble, the pressure by volume is given by:

$$p_i(T,\mu_i) = \frac{\theta\, g_i}{(2\,\pi)^3}\int d^3k \ln\left(1 + \theta\, e^{\beta(\mu - \epsilon(k))}\right), \tag{74}$$

where $\theta = \pm 1$ is given in according to the distribution, positive for fermions and negative for bosons. g_i is the degeneracy, $\beta = 1/T$, μ the being the potencial and $\epsilon(k) = \sqrt{k^2 + m^2}$. k is the wave number and m the mass.

How the chemical potential is constant, we can rewrite the equation (74) as follow:

$$p_i(T,\mu_i) = \frac{\theta\, g_i}{(2\,\pi)^3}\int d^3k \ln\left(1 + \theta\, e^{\beta\,\mu}\, e^{-\beta\,\epsilon(k))}\right). \tag{75}$$

We can reduce the integral in the (75) and use the aproximation for the logarithm $\ln\left(1 + e^x\right) = -\sum \frac{(-1)^n\,(e^x)^n}{n}$:

$$p_i(T,\mu_i) = \frac{\theta\, g_i}{(2\,\pi)^3}\int_0^\infty -\sum \frac{(\pm\,1)^{(n-1)}\, e^{n\,\beta\,\mu}\,(e^{\beta\,\epsilon(k)})^n}{n} 4\pi\,\frac{k^2}{\beta} dk \tag{76}$$

Organizing we have:

$$p_i(T,\mu_i) = \frac{\theta\, g_i}{(2\,\pi^2)\,\beta}\sum_{n=1}^{+\infty}\frac{(\pm\,1)^{(n-1)}}{n}\, e^{n\,\beta\,\mu}\int_0^\infty e^{n\,\beta\,\epsilon(k)} k^2 dk \tag{77}$$

Using $\epsilon(k) = \sqrt{k^2 + m^2}$ and $\beta = 1/T$ we rewrite the equation (78) as follow:

$$p_i(T,\mu_i) = \frac{\theta\, g_i}{(2\,\pi^2)}\,T\sum_{n=1}^{+\infty}\frac{(\pm\,1)^{(n-1)}}{n}\, e^{n\,\beta\,\mu}\int_0^\infty k^2 dk\, e^{n\,\frac{\sqrt{k^2+m^2}}{T}} \tag{78}$$

Doing the substitution $x = k/m$ we can write:

$$p_i(T,\mu_i) \approx g_i\,\frac{T^2\,m^2}{2\,\pi^2}\, e^{\frac{\mu}{T}}\, K_2\Big(\frac{m}{T}\Big) \tag{79}$$

Using the thermodynamics relations we can write the expressions for ϵ, n, and s for the i-nt particle as:

$$e_i(T,\mu_i) \approx g_i\,\frac{T\,m^3}{2\,\pi^2}\,e^{\frac{\mu}{T}}\Big[K_1\Big(\frac{m}{T}\Big)+\frac{3\,T}{m}\,K_2\Big(\frac{m}{T}\Big)\Big] \tag{80}$$

$$n_i(T,\mu_i) \approx g_i\,\frac{T\,m^2}{2\,\pi^2}\,e^{\frac{\mu}{T}}\,K_2\Big(\frac{m}{T}\Big) \tag{81}$$

$$s_i(T,\mu_i) \approx g_i\,\frac{T\,m^3}{2\,\pi^2}\,e^{\frac{\mu}{T}}\Big[K_1\Big(\frac{m}{T}\Big)+\frac{(4\,T-\mu_i)}{m}\,K_2\Big(\frac{m}{T}\Big)\Big]. \tag{82}$$

The results bellow give us the thermodynamical relations for the hadron gas. Although, Yen, Greiner and Yang (YEN M. I. GORENSTEIN,) shown those results should have a correction in order to fit the total particle number density. The correction in the volume are given given by:

$$P^{(ex)}(T,\mu_i) = \sum_{i=1}^{h} P_H(T,\hat{\mu}) \tag{83}$$

and the following identities for entropy, density number and energy are:

$$e_i^{(ex)}(T,\mu_i) \equiv \frac{\sum_{i=1}^{h} s_i(T,\hat{\mu})}{1+\sum_{j=1}^{h} v_j n_j(T,\hat{\mu})} \tag{84}$$

$$n_i^{(ex)}(T,\mu_i) \equiv \frac{\sum_{i=1}^{h} s_i(T,\hat{\mu})}{1+\sum_{j=1}^{h} v_j n_j(T,\hat{\mu})} \tag{85}$$

$$s^{(ex)}(T,\mu_i) \equiv \frac{\sum_{i=1}^{h} s_i(T,\hat{\mu})}{1+\sum_{j=1}^{h} v_j n_j(T,\hat{\mu})}. \tag{86}$$

Those relations complete the description of the hadronic phase.

2.5.3 QCD on the lattice EoS

This section is devoted to a brief introduction to the quantum chromodynamics (QCD) on the lattice. First of all we should say that we will only show this EoS on the practical side, aiming the use of it in the CHESS code. To a physical content we recommend the some literature (GATTRINGER, 2010).

The main idea in this EoS proposed by Huovinen and Petreczky (HUOVINEN; PETRECZKY, 2011) is to use a parametrization for QCD on the lattice for high temperature regime, and the hadron gas for a low temperature regime using the trace anomaly.

We know the trace of the energy-momentum tensor of a photon is null. But in QCD, the theory for quarks and gluons, this trace isn't null, this why that trace anomaly is called like this.

The expression used for trace anomaly is given by:

$$\Theta(T) = \epsilon(T) - 3P(T), \tag{87}$$

for ϵ being the energy density and P the pressure.

We can express the pressure difference between the range of temperature (T_{low}, T) using the trace anomaly as follow:

$$\frac{P(T)}{T^4} - \frac{P(T_{low})}{T_{low}^4} = \int_{T_{low}}^{T} \frac{dT'}{T'^5}\Theta(T). \tag{88}$$

Now we will introduce two parametrizations,one for high temperature regime and another for a low temperature. In a high temperature regime, $T > 250MeV$, the EoS used is the QCD, and the parametrization for the trace assume the form:

$$\frac{\Theta(T)}{T^4} = \frac{d_2}{T^2} + \frac{d_4}{T^4} + \frac{c_1}{T^{n_1}} + \frac{c_2}{T^{n_2}}, \tag{89}$$

where d_2, d_4, c_1, c_2, n_1, and n_2 are constant which can be evaluated according to (HUOVINEN; PETRECZKY, 2011). One can find three different values for the set of those constants, and those differents values regarding information about the peak in the plot $\Theta(T)/T^4$ vs. T.

The 3 approaches are labeled s95p-v1, s95n-v1, and s90f-v1. The number 95 and 90 indicates the percentage of $\Theta(T)$ reached at $T - 800MeV$, and letters p, n, and f indicates the specific treatment in the peak.

For a low temperature regime, $T < 184$, we use the following parametrization:

$$\frac{\Theta(T)}{T^4} = a_1\,T + a_2\,T^3 + a_3\,T^4 + a_4\,T^{10}, \tag{90}$$

where a_1, a_2, a_3 and a_4 are constants.

Once we have in hands the parametrization of trace anomaly in high and low temperature regime we can use equations (89) and (90) in order to get an expression for the pressure of QGP. First, replacing (90) in (88) we have:

$$\frac{P_H(T)}{T^4} - \frac{P(T_0)}{T_0^4} = \int_{T_0}^{T} \frac{dT'}{T'}\,(a_1\,T + a_2\,T^3 + a_3\,T^4 + a_4\,T^{10})$$

$$\frac{P_H(T)}{T^4} = \frac{P(T_0)}{T_0^4} + \int_{T_0}^{T} \frac{dT'}{T'}\,(a_1\,T' + a_2\,T'^3 + a_3\,T'^4 + a_4\,T'^{10})$$

$$\Longrightarrow\; P_H(T) = T^4\Big[\frac{P(T_0)}{T_0^4} + \int_{T_0}^{T}(a_1 + a_2\,T'^2 + a_3\,T'^3 + a_4\,T'^9)dT'\Big]. \tag{91}$$

Now, using (89) in (88) we have:

$$\frac{P_{QGP}(T)}{T^4} - \frac{P_H(T)}{T_H^4} = \int_{T_H}^{T} \frac{dT'}{T'}\,(\frac{d_2}{T'^2} + \frac{d_4}{T'^4} + \frac{c_1}{T'^{n_1}} + \frac{c_2}{T'^{n_2}})$$

$$\frac{P_{QGP}(T)}{T^4} = \frac{P_H(T)}{T_H^4} + \int_{T_H}^{T} (\frac{d_2}{T'^3} + \frac{d_4}{T'^5} + \frac{c_1}{T'^{n_1+1}} + \frac{c_2}{T'^{n_2+1}})\,dT'$$

$$\implies P_{QGP}(T) = T_H^4 \Big[\frac{P_H(T)}{T_H^4} + \int_{T_H}^{T} \big(\frac{d_2}{T'^3} + \frac{d_4}{T'^5} + \frac{c_1}{T'^{m_1+1}} + \frac{c_2}{T'^{m_2+1}}\big)\, dT'\Big]. \tag{92}$$

Equation (92) is the total pressure for the QGP in the interval $T_H < T < 800MeV$.

2.5.4 First Order (EoS)

The FO-EoS has a phase transition evolving both EoS, QGP and HG, as we wrote earlier. In this transition phase region we can equalized the EoS of both phases in order to get:

$$P_H(T, \mu) = P_{QGP}(T, \mu). \tag{93}$$

We show in figure Figura 4 the phase diagram evolving the QGP and HG:

Figura 4 – Phase transition

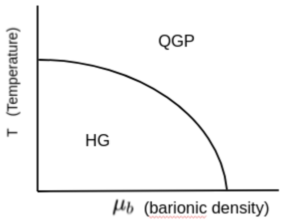

Font: Author's production.

The μ_b in figure Figura 4 represents the barionic density and T the temperature. The line between HG and QGP indicates special values of (T, μ_b) which defines a mixed phase where the equation (93) is valid.

An important remark is the following: the FO-EoS is one of the most simple description for the hydrodynamic evolution. In fact, we will use and describe near in the future better descriptions according to the experimental data such as lattice QCD (LQCD), AdS/QCD and quasiparticle model.

3 OBSERVABLES

In this section we are going to describe the observables. The observables are quantities which give us experimental measures generated in the particle accelerators. The first observable that we are going to describe is the rapidity and pseudorapidity distributions. Those quantities are related to the kinematic condition of the detected particle. After that we will describe the transversal momentum, or multiplicity. Finally we will describe the so-called flow harmonics, specially the elliptic flow, the most important observable in the RHIC which tell us how much anisotropically the energy can be distributed.

3.1 RAPIDITY & PSEUDORAPIDITY

In order to discuss those observables, we will start with the rapidity y. The rapidity y is used to describe the kinematic condition of a particle, and its mathematical description is given by:

$$y = \frac{1}{2} \ln \left(\frac{E + p_z}{E - p_z} \right), \tag{1}$$

where E is the energy and p_z refers to the momentum in the z-component or longitudinal momentum.

We can see the dependence of the energy in the rapidity description in equation . In the context of RHIC, it's more convenient to avoid to have a variable which describes kinematic condition of a particle with energy dependence. In this context, we introduce the pseudorapidity variable η given by the following equation:

$$\eta = -\ln \left[\tan \left(\frac{\theta}{2} \right) \right], \tag{2}$$

where θ is the relative angle between the particle to beam axis.

The pseudorapity variable is much more convenient because in RHIC we only can measure the angle of the detected particle relative to beam axis, and not its energy and longitudinal momentum.

In practice we have a large number of particles detected in the detector, so to describe the rapidity or pseudorapidity of all this particles we will consider a distribution N, for rapidity we use $\frac{dN}{dy}$ and for pseudorapidity $\frac{dN}{d\eta}$. Those quantities can be related, and the relation of rapidity and pseudorapidity is given by:

$$\frac{dN}{d\eta} = \sqrt{1 - \frac{m^2}{m_t^2 \cosh y}} \frac{dN}{dy}. \tag{3}$$

Rapidity and pseudorapidity distributions can be compared in the regions where the momentum $|p| >> m$, it implies in $\eta \approx y$

3.2 TRANSVERSE MOMENTUM DISTRIBUTION

The transverse momentum p_t is defined as the perpendicular momentum in the in relation to the beam momentum p_z. This quantity give us informations about the physical content of what happened in the collision process, once the initial momentum can be transfered.

Therefore it is natural to generalize this quantity to a distribution, once we are interested in the collective behavior. In terms of simulations, the transverse momentum distribution also give us information about the thermal decoupling of the system, and will be used to describe fit the experimental data together with the k_t parameter.

3.3 FLOW HARMONICS

The flow harmonics or collective flow, usually described using the letter v_i, give us informations about how the energy is distributed in space and the tool that we use for describe this flow is the hydrodynamics. The relation for the anisotropic flow is given by the expansion of the invariant triple differential distribution:

$$E\frac{d^3N}{d^3p} = \frac{1}{2\pi}\frac{d^2N}{p_t dp_t dy}\Big(1 + 2\sum_{n=1}^{\infty} v_n cos[n(\phi - \psi_{RP})]\Big), \tag{4}$$

where we identify E as the energy of the particle, p is the momentum, p_t is the transverse momentum, φ is the azimuthal angle, y is the rapidity,ψ_{RP} is the reaction plane angle, and the coefficients v_n are know as collective flow. Using the Fourier expansion we get the following expression for v_n:

$$v_n(p_t, y) =< cos[n(\phi - \psi_{RP})] > . \tag{5}$$

The brakets "<>"indicates an average over all particles, summed over all events. It is notorius the dependence of (p_t, y) in the harmonics. For each value of n we have a well determined coefficient. For $n = 1$ the coefficient is called as directed flow (v_1), $n = 2$ characterizes the elliptic flow (v_2). The elliptic flow is one of the most important observables in RHIC because it give us important information about how much anisotropically the energy is distributed and will be discussed soon. For $n = 3$ we have the triangular flow (v_3), $n = 4$ defines the quadrangular flow (v_4), and the last two are simply v_5, and v_6. The equation (5) is the method used in the Therminator 2 to compute the elliptic flow.

Also, please note the dependence of the angle to the reaction plane, which is not a direct observable (SMELLINGS,). Therefore we can also introduce another method to compute this quantity, called the reaction plane method.

Using this method, we have the relations for the Event plane given by:

$$Q_n^x = \sum w_i \cos(n\phi_i), \tag{6}$$

$$Q_n^y = \sum w_i \sin(n\phi_i), \tag{7}$$

where w_i is the weight of the i-nth particle and ϕ_i is the momentum azimuthal angle of produced particles in the laboratory system.

We can have the reaction plane angle ψ_{RP} computing:

$$\psi_{RP} = \frac{1}{n} \arctan\left(\frac{Q_n^x}{Q_n^y}\right). \tag{8}$$

With this description we can finally compute the elliptic flow in the reaction plane method using the following equation:

$$v_2 = \frac{\int_0^{2\pi} d\phi_p \cos 2(\phi_p - \psi_{RP}) \frac{d^3N}{p_t dp_t dy}}{\int_0^{2\pi} d\phi_p \frac{d^3N}{p_t dp_t dy}}. \tag{9}$$

Next section is devoted to present the numerical implementation that we used to compute all stages in the collisions.

4 NUMERICAL IMPLEMENTATION

We claim that our aim is to perform a numerical simulation in Relativistic Heavy Ion Collisions, and so far we did not explicitly show any information about the how we will do that. In this chapter we will describe the most important part of this work, the numerical implementation of the theory that we shown before in the last chapters.

In the first section of this chapter we will show the $T_R ENT_O$, a code regarding the collision process which uses a geometric model called Glauber model. Section 4.1 is devoted to VHLLE, the code which solves the hydrodynamics evolution of the system, i.e, will solve the equations of motion using the equations of state (EOS) specified.

In section 4.2 finally we will present the Therminator 2, which carries the decoupling of the hadrons via Cooper-Frye prescription. We also present in the final section the CHESS code, the main tool that we developed to unify those codes in such a smart way to reproduce all stages of RHIC.

We will discuss the scripts wrote in python which compose the CHESS code, and also show some modifications that we did in the code in order to have the final observables presented in the next chapter. Before we go ahead and introduce the codes itself, we may introduce the main idea which compose those codes during the space-time evolution.

In this context of the space-time evolution, it is important to describe how usually the codes developed to this goal in General Relativity or RHIC is implemented. We start the presenting the space-time foliation, i.e, we divide the the full space-time into the usual 3 spatial dimensions, and leave 1 dimension for the time component. In the 3D space, we assume a division of the full space in a set of 3D planes, and for one plane to another there will be a time evolution given by some step dt.

Figura 5 – Space-time Foliation

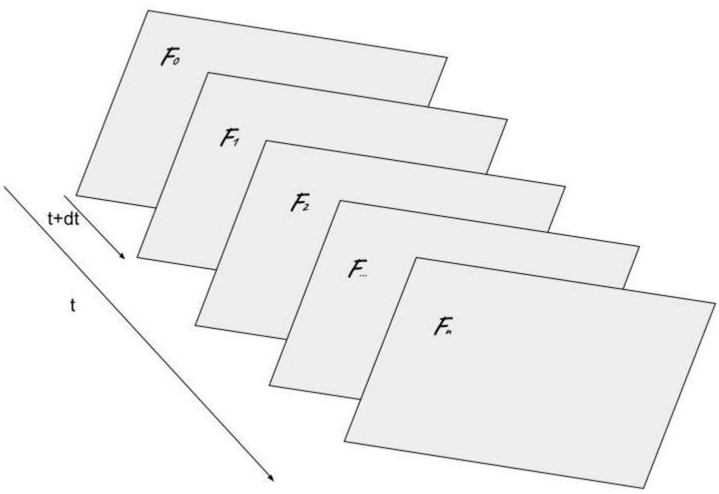

Font: Author's production.

In the figure Figura 5 we can the see the foliation. Each 3D plane F_i represents a unique system characteristic in a time t with some given quantities such as pressure, entropy, temperature, etc. To express the system evolution we change from some foliation, for example F_0 to F_1 using the time step dt.

This idea will be specially important when we will introduce the vHLLE in order to solve the equations of motion for relativistic hydrodynamics. Once we introduce the main idea we are able to go ahead and understand the numerical implementation used in our code.

4.1 $T_R ENT_O$

The Reduced Thickness Event-by-event Nuclear Topology ($T_R ENT_O$) is a numerical model to describe initial conditions for the collisions of p-p, p-n, and n-n with high energy using the Glauber Monte Carlo model (MORELAND J. C.; BERNHARD,).

We shown in section 2.1.1 that each projectile can be represented by the tickness function:

$$T_{AB}(x,y) = \int \rho_{AB}^{part}(x,y,z)dz, \tag{1}$$

where ρ_{AB}^{part} is the Woods-Saxon perfil given by:

$$\rho_{A,B}^{part}(x,y,z) = \frac{\rho_0}{1+\exp\left[\frac{(r-R_{A,B})}{a}\right]},$$

for a non-deformed nuclei, and:

$$\rho_{A,B}^{part}(x,y,z) = \frac{\rho_0}{1+\exp\left[\frac{(r-R_{A,B})(1+\beta_2 Y_{20}+\beta_4 Y_{40})}{a}\right]},$$

for a deformed nuclei.

The deformation factors β_2, β_4 are directly related to experimental measurements. Shou (SHOU Q.Y; MA,) present the deformation factor β_2 as a quantity derived from measurements of the reduced eletric quadrupole transition probability from the ground state 0^+ to the first 2^+ state given by the following relation:

$$\beta_2 = \frac{4\,\pi}{3\,Z\,R_0^2}\sqrt{\frac{B(E2)}{e^2}}, \tag{2}$$

where $R_0 = 1.2A^{1/3}$, for A being the nucleon number, Z the proton number, e the electron charge, and $B(E2)$ is obtained by:

$$B(E2) = \frac{5}{16\,\pi}\,|eQ_{20}|, \tag{3}$$

for Q_{20} being the intrinsic quadrupole moment evaluated as follow:

$$Q_{20} = \sqrt{\frac{16\,\pi}{5}}\int d^3r < \psi|r^2\,Y_{20}\,\rho(\vec{r})|\psi > . \tag{4}$$

This set of equations (2), (3), and (4) are not computed in the scope of $T_R ENT_O$. It assumes and use the experimental data.

We assume that: i) the eikonal approximation is valid and the entropy is produced if the thickness function of each participant T_A, T_B eikonally overlap. The eikonal approximation is a method to rewrite for example a partial diferential equation into a single variable, this reduction into a single variable allow us to chooce the straight line as special direction. ii) exist a scalar fiel $f(T_A, T_B)$ which converts the thickness intro entropy deposition.

The proposition for the scalar field f named reduced thickess is the following:

$$f(T_A, T_B) = T_R(p, T_A, T_B) = \Big(\frac{T_A^p + T_B^p}{2}\Big)^{1/p}, \tag{5}$$

where p is a dimensionless parameter.

The parameter p can be considered as a constant to differenciate different physical mechanism of entropy production, assuming values $-\infty < p < \infty$. The reduced thickness assume: $max(T_A, T_B)$ for $p \to \infty$, $min(T_A, T_B)$ for $p \to -\infty$, the arithmetic mean $(T_A + T_B)/2$ for $p = +1$, the geometric mean $\sqrt{T_A T_B}$ for $p = 0$, and the harmonic $2T_A T_B/(T_A + T_B)$ for $p = -1$.

The participants collide assuming the inelastic collisions, with probability given by:

$$P_{col}(b) = 1 - \exp\left[-\sigma_{gg} T_{pp}(b)\right], \tag{6}$$

where b is the impact parameter, σ_{gg} is the effective parton-parton cross section, and T_{pp} is:

$$T_{pp}(b) = \int T_p(x + b/2, y) T_p(x - b/2, y)\, dx\, dy, \tag{7}$$

is the nuclear thickness function.

The nuclear thickess T_p is given by the gaussian:

$$T_p(x, y) = \frac{1}{2\,\pi\lambda^2} \exp\Big[-\frac{x^2 + y^2}{2\,\lambda^2}\Big], \tag{8}$$

with λ being the nucleon width.

The effective parton-parton cross section should be fixed in order to reproduce the inelastic cross section σ_{NN} given by:

$$\sigma_{NN} = \int 2\pi P_{col}(b)\, b\, db. \tag{9}$$

We know in the collision process not all nucleons interact, we are interested in the participant nucleons, so the following step is to define the nuclear thickness of the participants as follow:

$$T(x, y) = \sum_{i}^{N_{part}} w_i T_p(x - x_i, y - y_i). \tag{10}$$

The term w_i is the weight, is related to the gamma distribution:

$$P_k(w) = \frac{k^k}{\Gamma(k)} w_i^{k-1} e^{-k\, w_i}, \tag{11}$$

with k know as the shape parameter.

The weight w_i introduces fluctuations in the multiplicity, and k may be tuned in order to fit the data. For $0 < k < 1$ we have large multiplicity fluctuations, and $k >> 1$ suppress the fluctuations.

In summary, the most important $T_R ENT_O$ input parameters are k, λ, p, k_t, and w. w is the weight and k is the fluctuation, both can be related as we can see in equation (11). The parameter λ has a geometric meaning, the nucleon width. The parameter p interpolates and lead us to different entropy deposition mechanism. The k_t parameter was implemented in order to fit the multiplicity according to the experimental data.

$T_R ENT_O$ will be an important tool to test a range of nuclei assuming a set of degrees of freedom of deformation factors β_2, and β_4 for deformed nuclei implemented using the deformed Woods-Saxon perfil.

sectionVHLLE

In this section we will describe hydrodynamical evolution implemented by the vHLLE. The viscous Harten-Lax-van Leer-Einfeldt (vHLLE) describe the evolution of the system (HUOVINEN P.; BLEICHER,), which is governed by the equations of state.

From the theory presented in the section 2.3 we know the equations of relativistic hydrodynamics are given by the conservation of energy-momentum tensor and charge current:

$$\partial_\nu T^{\mu\nu} = 0, \tag{12}$$

$$\partial_\nu N_c^\mu = 0, \tag{13}$$

for $T^{\mu\nu}$ being the energy-momentum tensor and N_c^μ the charge current, and c be each conserved charges. Both equations are valid to ideal or viscous hydrodynamics.

In order to solve those equation numerically, we rewrite those relations as:

$$\frac{\partial Q^\mu}{\partial t} + \frac{\partial F^{\mu i}}{\partial x_i} = 0, \tag{14}$$

$$\frac{\partial N^0}{\partial t} + \frac{\partial N^i}{\partial x_i} = 0, \tag{15}$$

assuming i is the spatial dimensions, $T^{0\mu} = Q^\mu$, and N_0 being conserved quantities.

The code uses the finite volume method to solve the equations (14), and (15). Integrating (14), and (15) for $[t_n, t_n + \Delta\, t]$ and $[x_i - \Delta x/2, x_i + \Delta x/2]$ we have the relation between the conserved quantities and the fluxes:

$$\frac{1}{\Delta t}(Q_i^{n+1} - Q_i^n) + \frac{1}{\Delta x_i}(F_{i+1/2}^n - F_{i-1/2}^n) = 0. \tag{16}$$

The last equation is used to propagate Q^n to the next timestep and it is a representation of ideal hydrodynamics. For the viscous hydrodynamics the relation for conserved quantities and the fluxes are given by:

$$\frac{1}{\Delta t}(Q^{n+1}_{Id,i} + \delta\, Q^{n+1}_{i} - Q^{n}_{Id,i} - \delta\, Q^{n}_{i}) + \frac{1}{\Delta x_i}(\Delta\, F_{Id} + \Delta\, \delta F) + S_{Id,i} + \delta\, S_i = 0, \tag{17}$$

where we identify $\Delta F = F_{i+1/2} - F_{i-1/2}$, and terms with δ indicates viscous corrections, and S is the source term. From equation (17) is possible to write two equations, separating the ideal and viscous corrections.

The code use 3 substeps for evaluate the solution of the equation (17): i) use the ideal part of energy-momentum tensor for Δt for find Q^{*n+1}_{Id}; ii) Solve the Israel-Stewart equations to propagate $\pi^{\mu\nu}$ and Π; iii) Obtain $Q^{n+1}_{full} = Q^{n+1}_{Id,i} + \delta\, Q^{n+1}_{i}$ using equation (17).

4.2 THERMINATOR 2

This section is devoted to descibre the THERMal heavy IoN generATOR 2 (THERMINATOR 2) a numerical code which use the Monte Carlo approach to generate events and study the statistical production of particles in RHIC (CHOJNACKI M. LAJ; KISIEL, 2002) using the freeze-out surface. The THERMINATOR 2 evaluat the total emitted particles using the equation:

$$N = \int dy\, p_T\, dp_T\, d\phi_p \int_{\Sigma} d\Sigma_\mu\, p^\mu\, f(x,p), \tag{18}$$

where y is the rapidity, p_t is the transverse momentum given by the relation $p_t = \sqrt{p_x^2 + p_y^2}$, the $\phi_p = \arctan\,(p_y/p_x)$ is the momentum azimuthal angle, and $f(x,p)$ is the distribution function. As we mentioned before, there is two different ways to parametrize the freeze-out hypersurface, using a 2+1D code, or using a 3+1D code. We will show both pametrizations:

For 2+1D codes, the parametrization of the hypersurface is given using the set of variables:

$$t = d(\phi,\zeta,\eta)\, \sin\zeta\, \cosh\eta$$

$$x = d(\phi,\zeta,\eta)\, \cos\zeta\, \cos\phi$$

$$y = d(\phi,\zeta,\eta)\, \cos\zeta\, \sin\phi$$

$$z = d(\phi,\zeta,\eta)\, \sin\zeta\, \sinh\eta$$

$$\eta = \tanh^{-1}\frac{z}{t}$$

$$\tau = d(\phi,\zeta,\eta)\, \sin\zeta \tag{19}$$

With this set of variables, we must compute the 4-momentum and the 4-velocity. The 4-velocity is given by:

$$u^\mu = \gamma_T(\cosh y_L, \tanh y_T\ \cos\phi, \tanh y_T\ \sin\phi, \sinh y_L), \tag{20}$$

with γ_T being the Lorentz factor in the transversal component, y_L the longitudinal rapidity and y_T the transversal rapidity.

The x, and y componente will be held untouched, so we should compute the transformation in τ and η as follow:

$$u^\tau = \frac{\partial\tau}{\partial t}\, u^\tau + \frac{\partial\tau}{\partial z}\, u^z, \tag{21}$$

$$u^{\eta_s} = \frac{\partial\eta_s}{\partial t}\, u^\tau + \frac{\partial\eta_s}{\partial z}\, u^z. \tag{22}$$

We know that:

$$\tau^2 = t^2 - z^2, \quad \text{and} \quad \eta_s = \frac{1}{2}\ln\frac{t+z}{t-z}, \tag{23}$$

but also we have:

$$t = \tau\cosh\eta_s \quad \text{and} \quad z = \tau\ \sinh\eta_s, \tag{24}$$

deriving we find:

$$\frac{\partial\tau}{\partial t} = \cosh\eta_s \qquad \frac{\partial\tau}{\partial z} = -\sinh\eta_s$$

$$\frac{\partial\eta_s}{\partial t} = \frac{1}{\tau}\ \sinh\eta_s \qquad \frac{\partial\eta_s}{\partial z} = \frac{1}{\tau}\ \cosh\eta_s \tag{25}$$

Now, using equations (21), and (22) together with components u^0 and u^3 we have:

$$u^\tau = \gamma_T\ \cosh\eta_s\ \cosh y_L - \gamma_T\ \sinh\eta_s\ \sinh y_L$$

$$\implies u^\tau = \gamma_T\ \cosh y_L - \eta_s, \tag{26}$$

and

$$u^{\eta_s} = \gamma_T\,\frac{1}{\tau}\sinh\eta_s\ \cosh y_L - \gamma_T\,\frac{1}{\tau}\cosh\eta_s\ \sinh y_L$$

$$\implies u^{\eta_s} = \frac{\gamma_T}{\tau}\ \sinh y_L - \eta_s. \tag{27}$$

Once we have equations (26), and (27) we can rewrite the 4-velocity as follow:

$$u^\mu = \gamma_T(\cosh(y_L - \eta_s), \tanh y_T\ \cos\phi, \tanh y_T\ \sin\phi, \frac{1}{\tau}\sinh(y_L - \eta_s)), \tag{28}$$

and using the relation $p^\mu = m\, u^\mu$ we can write the 4-momentum as:

$$p^\mu = \gamma_T(m_T\ \cosh(y_L - \eta_s), m_T\ \tanh y_T\ \cos\phi, m_T\ \tanh y_T\ \sin\phi, \frac{m_T}{\tau}\sinh(y_L - \eta_s)),$$

and how $p_T = m_t \tanh y_L$ we finally obtain an expression for the 4-momentum:

$$p^\mu = \gamma_T(m_T \cosh(y_L - \eta_s), p_T \cos\phi, p_T \sin\phi, \frac{m_T}{\tau}\sinh(y_L - \eta_s)). \tag{29}$$

Once we have the expression for the 4-momentmum p^μ, now we need an expression for $d\Sigma_\mu$ to complete the integral (18). From differential geometry we know that $d\Sigma_\mu$ assumes the form:

$$d\Sigma_\mu = \epsilon_{\mu\nu\alpha\beta}\frac{\partial x^\mu}{\partial\eta}\frac{\partial x^\alpha}{\partial\zeta}\frac{\partial x^\beta}{\partial\phi}d\eta\, d\zeta\, d\phi, \tag{30}$$

for $\epsilon_{\mu\nu\alpha\beta}$ being the four dimensional Levi-Civita symbol.

The computation of each component of $d\Sigma_\mu$ is not straightforward and we will left it in blank giving only the complete expression $d\Sigma_\mu\, p^\mu$ as follow:

$$\begin{aligned} d\Sigma_\mu\, p^\mu = d^2\sin\zeta\Big[d\cos\zeta(m_T\sin\zeta\cosh(\eta - y) + p_T\cos\zeta\cos(\phi - \phi_p)) + \\ + \frac{\partial d}{\partial\zeta}\cos\zeta(-m_T\cos\zeta\cosh(\eta - y)) + p_T\sin\zeta\cos(\phi - \phi_p) + \\ \frac{\partial d}{\partial\phi}p_T\sin(\phi - \phi_p) + \frac{\partial d}{\partial\eta}\cot\zeta\, m_T\sin(\eta - y)\Big]. \end{aligned} \tag{31}$$

Equation (31) together with the further description of distribution function completes the integral (18) for 2+1D codes. The symmetry in this set of parametrization is boost-invariant. One can find also 2+1D codes using the cylindrical symmetry (CHOJNACKI M. LAJ; KISIEL, 2002).

We parametrize in the 3+1D code the freeze-out hypersurface Σ using the coordinates τ, x, y, η_s as follow:

$$\tau = \tau_0 + d(\zeta, \varphi, \theta)\sin\theta\cos\zeta$$

$$x = d(\zeta, \varphi, \theta)\sin\theta\cos\zeta\cos\varphi$$

$$y = d(\zeta, \varphi, \theta)\sin\theta\cos\zeta\sin\varphi$$

$$\eta_s = d(\zeta, \varphi, \theta)\cos\theta, \tag{32}$$

where τ_0 is the initial time, and $d(\zeta, \varphi, \theta)$ is a distance between origin to the some given point in the hypersurface.

In this new coordinate system (τ, x, y, η_s), we should compute each component of $d\Sigma_\mu = (d\Sigma_0, d\Sigma_1, d\Sigma_2, d\Sigma_3)$, following the same approach used in 2+1D parametrization.

The $d\Sigma_\mu$ will be given by the set of equations:

$$d\Sigma_0 = d^2\tau\sin\theta\cos\zeta\Big(\Big[d\sin\theta - \frac{\partial d}{\partial\theta}\cos\theta\Big]\sin\theta\sin\zeta - \frac{\partial d}{\partial}\cos\zeta\Big)d\theta\, d\zeta\, d\varphi \tag{33}$$

$$
\begin{aligned}
d\Sigma_1 = d^2\tau\, \sin\theta \Big(\Big[& d\cos^2\zeta \sin^2\theta \cos\varphi + \frac{\partial d}{\partial \varphi} \sin\varphi + \cos\zeta \cos\varphi \\
& \Big(\frac{\partial d}{\partial \zeta} \sin\zeta - \frac{\partial d}{\partial \theta} \cos\theta \sin\theta \cos\zeta \Big) \Big] d\theta\, d\zeta\, d\varphi
\end{aligned} \tag{34}
$$

$$
\begin{aligned}
d\Sigma_2 = d^2\tau\, \sin\theta \Big(\Big[& d\cos^2\zeta \sin^2\theta \sin\varphi - \frac{\partial d}{\partial \varphi} \cos\varphi + \cos\zeta \sin\varphi \\
& \Big(\frac{\partial d}{\partial \zeta} \sin\zeta - \frac{\partial d}{\partial \theta} \cos\theta \sin\theta \cos\zeta \Big) \Big] d\theta\, d\zeta\, d\varphi
\end{aligned} \tag{35}
$$

$$
d\Sigma_3 = d^2\tau\, \sin^2\theta\, \cos\zeta \Big(d\cos\theta + \frac{\partial d}{\partial \theta} \sin\theta \Big)\, d\theta\, d\zeta\, d\varphi. \tag{36}
$$

Now we must compute the 4-momentum in the Milne coordinates and evaluating the multiplication in equation (18), leading us to the final expression:

$$
\begin{aligned}
d\Sigma_\mu\, p^\mu = d^2\tau \Big(& \frac{\partial d}{\partial \zeta}\, \cos\zeta [-m_t \cos\zeta \cosh(y - \eta_s) + p_t \sin\zeta \cos(\varphi - \phi_p)] \\
+ d\cos\zeta [m_t\, \sin\zeta \cosh(y - \eta_s) & + p_t \cos\zeta \cos(\varphi - \phi_p)] + \frac{\partial d}{\partial \phi}\, p_t\, \sin(\varphi - \phi_p) \Big).
\end{aligned} \tag{37}
$$

Equation (37) together with the distribution function will complete the integral in the equation (18), to complete the description for 2+1D or 3+1D codes we need to describe the distribution function $f(x, p)$.

In general, 3+1D codes doesn't have any symmetry related according to (CHOJNACKI M. LAJ; KISIEL, 2002). Also is important to mention that for 3+1D code or 2+1D code, the results won't be modified, hold the physics in both descriptions the same despite the system being different.

The most general form of distribution function includes a correction due to bulk and shear viscosity as follow:

$$
f(x, p) = f_0(x, p) + \delta\, f_\pi(x, p) + \delta\, f_\Pi(x, p), \tag{38}
$$

for $f_0(x, p)$ being the distribution function at the equilibrium, $\delta\, f_\pi(x, p)$ is related to the shear viscosity, and $\delta\, f_\Pi(x, p)$ to the bulk viscosity. It's clear that if we assume the ideal hydrodynamics there is no correction in $\delta\, f_\pi(x, p)$ and $\delta\, f_\Pi(x, p)$, the terms are identically null and the expression (38) assumes the simple form $f(x, p) = f_0(x, p)$.

The equilibrium distribution function f_0 obey the relation:

$$
f_0(x, p) = \frac{g}{(2\pi)^3} \frac{1}{\exp\left[\frac{p_\mu u^\mu - \mu}{T_{fo}}\right] \pm 1}, \tag{39}
$$

where g is the degenerescence, T_{fo} is the freeze-out temperature, p_μ the four-moment, u^μ the four-velocity, and μ the chemical potential. The symbol $\pm$ indicates if we are using fermions or bosons.

In our case we assume that the chemical potencial $\mu = 0$ due to fact in the EoS that we are using has null barionic density. We can write the multiplication in the exponential as:

$$p_\mu \, u^\mu = \frac{1}{\sqrt{1 - v_t^2}} (m_t \, \cosh(y - \eta_s) - v_t \, p_t \, \cosh(\varphi - \phi_p)), \tag{40}$$

which was obtained using the Milne coordinates. In the viscous case, the shear and bulk viscosty correction are given by the expressions:

$$\delta f_\pi(x,p) = f_0(x,p)[1 \pm f_0(x,p)] \, \frac{1}{2 \, T_{fo}^2 \, (\epsilon + P)} \, p^\mu \, p^\nu \, \pi_{\mu \, \nu} \tag{41}$$

$$\delta f_\Pi(x,p) = \frac{1}{C} \, f_0(x,p)[1 \pm f_0(x,p)] \left(\frac{(u^\mu \, p_\mu)^2}{3 \, u^\mu \, p_\mu} - c_s^2 \, u^\mu \, p_\mu \right) \Pi, \tag{42}$$

where we identify: ϵ as the energy density, P the pressure and $\pi_{\mu\,\nu}$ the shear viscosity tensor, c_s the sound velocity, Π the bulk viscosity, and C is given by:

$$C = \frac{1}{3} \sum_{i=1}^{h} \int \frac{d^3 p}{(2\,\pi)^3} \, \frac{m^2}{E} \, f_0(x,p) \, [1 \, \pm \, f_0(x,p)] \left(\frac{p^2}{3E} - c_s^2 \, E \right), \tag{43}$$

with E, and m being energy and mass of each particle. The sum must occurs over all hadrons. The equations (37), (39), (41), and (42) together with the equation of state (EOS) presented in section 2.5 completes the decoupling criterion of the system, solving equation (18) in 3+1D parametrization for freeze-out hypersurface. Analogously, equations (31), (39), (41), and (42) together with the equation of state (EOS) completes the description for 2+1D parametrization for freeze-out hypersurface.

In this work, we will use in all simulations the 2+1D parametrization. Another important tool used in the THERMINATOR is the decayment. The decayment is described by the cascade model, illustrated in the figure below:

Figura 6 – Cascade Model

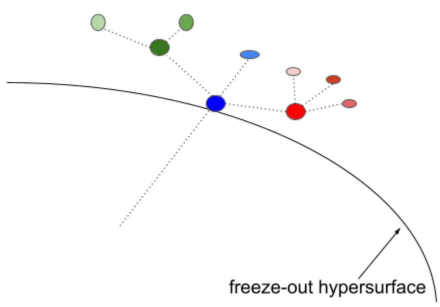

Font: Author’s production.

In the figure Figura 6, we can see the scheme of the cascade model. A single hadron, represented by the blue circle travel and pass through the freeze-out surface. It decouples in three particles, represent by smallest blue one, red and green. Posteriorly those particles also can decay in another particles, the green and red ones. This is the reason that the model is named as cascade model.

In this model, the direction and the momentum of each particle are determined randomly. The particles implement in the code come from the particle data group (PDG), and contains all information about the name, spin, mass, width, and others characteristics from the direct particle or daughters particles.

In the next section we will present the CHESS code and how it is useful in the RHIC description.

4.3 CHESS

The Complete Hydrodynamical Evolution SyStem (CHESS) code is a script written in python originally by Dener Lemos, a collaborator from the IFT-UNESP, under test and modified by our group. The script evolves the three codes mentioned ealier, the $T_R ENT_O$ which regards informations of initial conditions, the vHLLE for the hydrodynamical evolution, and the THERMINATOR 2 for the decoupling stage.

The code provide different nuclei, implemented in $T_R ENT_O$ by Woods-Saxon perfil, and different kinds of EoS, which can be used to compare the effect of EoS, initial conditions, and freeze-out temperature in the observables.

The main idea of the code is to give a complete description to the hydrodynamical systems without any further deep knowledge in programming. In figure Figura 7 we present the CHESS code flowchart.

Figura 7 – CHESS flowchart

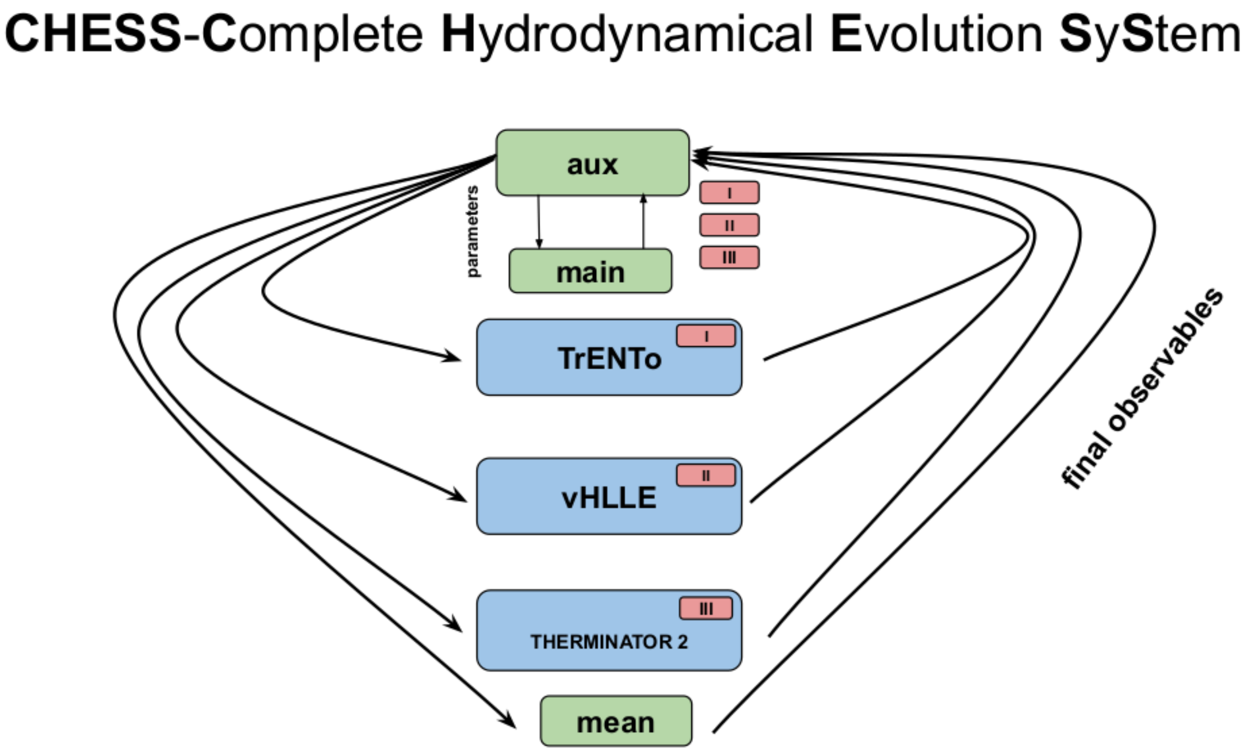

Font: Author's production.

In the flowchart, the green boxes represents the scripts written in python, while blue boxes are well-known codes used in numerical simulations in RHIC, and rosé boxes are input files. The CHESS code uses an initial input parameters file which contains the full information, or input parameters, for each code. With this information, the aux script will call the main, which will separate these information in three, described in rosé boxes I, II and III, and organize it in a proper folder for each code. Once the input files are prepared the main script finishes and turn to the main script.

The first code to be runned is $T_R ENT_O$. We will perform the computations on initial conditions and separate it in a systematic and organized way all IC for each event using the input parameters I obtained from aux. After the code complete the events generation, it turns back to the aux and the system is prepared to the space-time evolution, described by the hydrodynamical model.

The aux will call the vHLLE code which use the input parameters II. The vHLLE code will be executed according to the type of IC, one time if the IC is smooth, or NE times if the IC is event-by-event type. NE is the number of events defined in the CHESS input parameter file. After the hydrodynamical model is complete, the outputs file will be organized by the script, it turns back again to the aux script and the system is prepared to the final stage.

One of the last steps is to run the THERMINATOR 2 with the input parameter III in order to obtain the observables. Once the decoupling is done, the code turns back to the aux. The aux finally will call the mean, the final step. In this part the mean script will compute the mean of all observables according to the IC. We will describe explicitly in the next subsection the modifications which we did in the CHESS code to contribute in our collaboration.

4.3.1 Modifications

The first contribution we made was in organize an arrangement to set the environment on the grid-UNESP to run the code. In principle when we receive the code, it is not working due to conflicts with system libraries.

The effective changes we made in the code are the following: In its first version, when the script try to run the vHLLE inside the loop of hydrodynamical evolution, using NE> 4, for some unknown reason there is some missing events and the vHLLE cannot return a proper ouput file, and it generate a fail in the code and we cannot compute all system. In order to solve this error, we include a test to check the existence or not of those output file, and with that we can generalize the code to a generic NE.

Another essential modification we made is the inclusion of the proper resolution factor R_n in the macro used to plot the elliptic flow. In principle, higher values of $R_n > 1$ implies in a low values of the elliptic flow v_2 when we compare to the experimental data. If we use a low resolution factor, $R_n < 0.8$ it will lead to a high elliptic flow v_2 compared to the experimental data. We include the resolution factor $R_n = 0.99$, according to the results found in the THERMINATOR 2.

The future plan is to turn the code public once we finish the test phase. In the next chapter we will present the results that we obtain using the CHESS code.

5 RESULTS

In this section we will show the results obtained so far using the CHESS code described in the section 4. We mention before that our aim is to study the effect of the deformed nuclei in the observables, specially the collective flow. We started this study with a set with 5 types of nuclei as follow: three types of deformed uranium named U, U2, and U3, and one symmetric gold (Au) nuclei, and one deformed Au nuclei, named Au2.

The information related to each nuclei was implemented via Woods-Saxon perfil shown in the section 2.1.1. In principle, the parameters related to the Woods-Saxon perfil for each nuclei is presented below:

Tabela 1 – Different nuclei implemmented in T_RENT_O

Symbol	R	a	β_2	β_4
U	6.81	0.60	0.280	0.093
U2	6.86	0.42	0.265	-
U3	6.67	0.44	0.280	0.093
Au	6.37	0.535	-	-
Au2	6.37	0.60	-0.131	-0.031

Font: Author's production.

Table 1 shown to us the original nuclei implemented in T_RENT_O. With this in mind we propose a new set of nuclei, based on those experimental data and including a symmetric nuclei for each uranium nuclei implemented. In fact, we propose a set of variations in the deformation factors for each nuclei in order to see the effect of those deformations in the final observables.

Firstly, to see the behavior of the Woods-Saxon perfil subjected under those deformation factors, we did an implementation using root-CERN using the Woods-Saxon perfil equations (2), and (2), the results are presented below:

Figura 8 – Woods-Saxon Perfil for Au+Au nuclei

Font: Author's production.

In all figures above, the red line represents the symmetric nuclei, the black one represents the full deformed nuclei which includes the parameters β_2, and β_4, and the purple line (when it is draw) represents the deformed nuclei subjected only to the β_2 factor.

One can see for Au nuclei, the effect of the deformation factors (β_2, β_4) in the Woods-Saxon perfil is relatively small when it is compared to the symmetric nuclei. On the other side, in uranium nuclei we will see a different behavior comparing symmetric and deformed nuclei as follow:

Figura 9 – Woods-Saxon Perfil for U+U nuclei

Font: Author's production.

Figura 10 – Woods-Saxon Perfil for U2+U2 nuclei

Font: Author's production.

Figura 11 – Woods-Saxon Perfil for U3+U3 nuclei

Font: Author's production.

As mentioned ealier, we can see a difference between deformed and symmetric nuclei, specially for U and U3 nuclei. The curves which regard information about the deformation factors explicity appears as a deviation from the symmetric nuclei. It show to us clearly the effect of the deformation factors in the Woods-Saxon perfil.

We also can construct those arguments in the assigned values of the deformation factors, (β, β_4), specially if we compared Au and U data. Based on that, we did some modifications in the $T_R ENT_O$

code, implementing all those symmetric and deformed nuclei, and also we will present some tests increasing or decreasing the values of the deformation factors.

In the table 2, we will present the implementation that we propose and modify in T_RENT_O:

Tabela 2 – New nuclei implemmented in T_RENT_O

Symbol	R	a	β_2	β_4
$U(\beta_2, \beta_4)$	6.81	0.60	0.280	0.093
$U(\beta_2)$	6.81	0.60	0.280	-
U_s	6.81	0.60	-	-
$U2(\beta_2, \beta_4)$	6.86	0.42	0.265	-
$U2_s$	6.86	0.42	-	-
$U3(\beta_2, \beta_4)$	6.67	0.44	0.280	0.093
$U3(\beta_2)$	6.67	0.44	0.280	-
$U3_s$	6.67	0.44	-	-
Au	6.37	0.535	-	-
$Au2(\beta_2, \beta_4)$	6.37	0.60	-0.131	-0.031
$Au3(\beta_2)$	6.37	0.60	-0.131	-

Font: Author's production.

According to the reference (ADAMCZYK,), the collisions between deformed gold and uranium can be used to study how particle production and the azimutal anisotropy can be affected according to the nuclei initial geometry. For charged hadrons the pseudorapidity distribution for experimental data in Au+Au at $\sqrt{S_{NN}} = 200GeV$ and U+U at $\sqrt{S_{NN}} = 193GeV$ collisions can be parametrized as follow:

$$\left(\frac{dN_{ch}}{d\eta}\right)^{1/4} = c_1 - c_2\, x + c_3\, \exp\left(-c_4\, x^{c_5}\right), \tag{1}$$

where c_i are constants with values: $c_1 = 5.3473$, $c_2 = 4.298$, $c_3 = 0.2959$, $c_4 = 18.21$, and $c_5 = 0.4541$ for U+U and $c_1 = 5.0670$, $c_2 = 3.923$, $c_3 = 0.2310$, $c_4 = 18.37$, and $c_5 = 0.4842$ for Au+Au.

With those nuclei given in table 2, and the parametrization for experimental data from STAR (1) we start a search for the T_RENT_O initial conditions which minimizes the chi-squared test, according to the (GIACALONE,) in order to reproduce the experimental data from the STAR collaboration (ADAMCZYK,). We are looking for the parameters p, k and w which minimizes the χ^2.

The chi-squared test tests the quality of fitness, or how good the assumed hypothesis is according to the experimental data. Visually the test show how approximate your assumption is from the theoretical value, if the $\chi^2 < 1$, indicates your assumption has good according to the theoretical data, if $\chi^2 >> 1$ your assumption cannot be considered reasonably according to the theory and must be despised. The test follows the following relation:

$$\chi^2 = |O^2_{measured} - O^2_{expected}|, \tag{2}$$

where $O_{measured}$ is the measured value, and $O_{expected}$ is theoretical value for the test. In our case the T_RENT_O will be used as measured value while the data from STAR collaboration will be the expected value.

We vary the T_RENT_O input parameters in the range: $-2 \leq p \leq 2, 0 \leq k \leq 2$, and $0.2 \leq w \leq 0.6$ with a step equal to 0.1 generating thousands of events, and implement the chi-squared test in the ROOT, a data analysis tool developed by the CERN, and implemented in $C++$ language, widely used by high energy physics, particle physics, and so on, and the parametrization (1) plotting $\left(\frac{d(dN/d\eta)}{dc}\right)^{-1}\Big|_c vs. \frac{dN_{ch}}{d\eta}\Big|_c$ where $c \in [0,1]$ is the centrality.

The centrality is defined as the cumulative of multiplicity:

$$c(dN/d\eta) = \int_{dN/d\eta}^{\infty} P(dN/d\eta), \tag{3}$$

where $P(dN/d\eta)$ is the probability density. Deriving the inverse of this relation we obtain the probability density.

For each of those set of parameters p, k, and w we found a minimum value for the χ^2, and from this approximated values of (p, k, w) we did a new search, varying the parameters around those approximated values with the step equal to 0.01, in order to find a more accurate value.

We show in Figura 12 the result of the minimum χ^2-test containing the $T_R ENT_O$ results and the parametrization for the experimental data from STAR collaboration for each nuclei, where the blue star represents the STAR collaboration data obtained from the reference (ADAMCZYK,), and the red circle represents the $T_R ENT_O$ data.

Figura 12 – χ^2-test in different nuclei collisions.

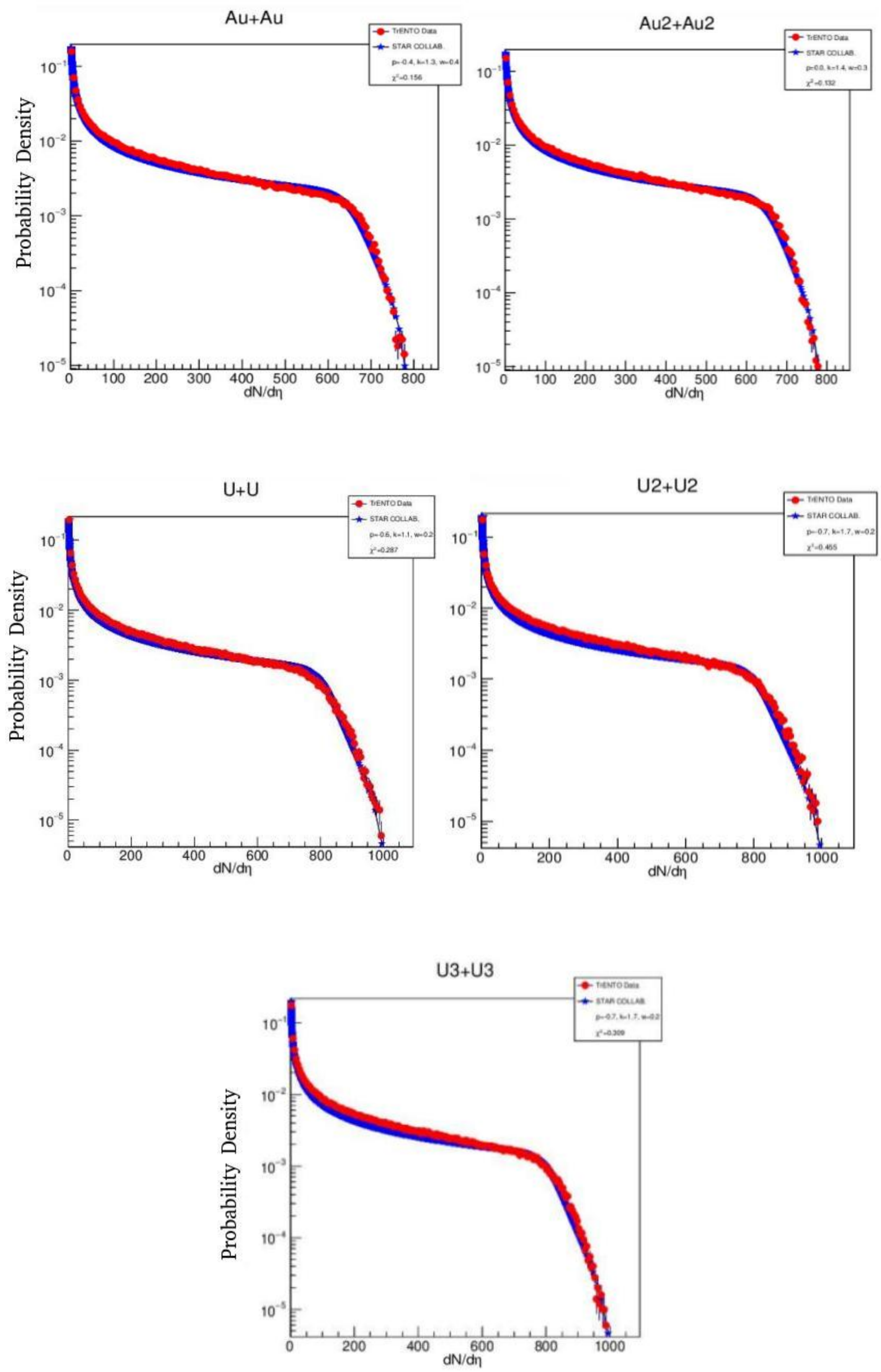

Font: Author’s production.

We show in the table 3 a summary with the values obtained for T_RENT_O input parameters p, k, and w for symmetric and deformed Au and U nuclei according to the minimization evaluated as well the result of the χ^2-test.

Tabela 3 – $T_R ENT_O$ optimized input parameters

Nuclei	p	k	w	χ^2
Au	-0.4	1.3	0.4	0.156
Au2	0.0	1.4	0.6	0.132
U	-0.6	1.1	0.2	0.287
U2	-0.7	1.7	0.2	0.455
U3	-0.7	1.7	0.2	0.309

Font: Author's production.

Those set of parameters in table 3 will be used as an initial condition to run the CHESS code. In the next sections we will show the results regarding all those set of nuclei. Firstly we will present the results regarding the FO-EoS, using the ideal hydrodynamics.

5.1 IDEAL HYDRODYNAMICS

This section is devoted to present the results obtained using the CHESS code for the ideal Hydrodynamics. We will start the presentation of the results with the particle distribution. It is important to mention the fact the particle distribution is the most easy observable to be obtained, even with a small number of events, NE=100 for example, in general, is good enough to reproduce the experimental data.

We will present in the following subsections the results regarding the Au and U nuclei, showing the initial conditions beyond the particle distributions, the collective flow, v_2, and v_4 which is the aim of this study.

5.1.1 Gold nuclei

For gold nuclei, before go ahead and show the observables, we will present the results related to the initial conditions obtained via $T_R ENT_O$. Table 4 present the results related to initial conditions of Au+Au collisions:

Tabela 4 – Au+Au collisions initial conditions

b	9.779
N_{part}	105
e_2	0.428
e_4	0.348

Font: Author's production.

From table 4, we identify b as being the impact parameter, N_{part} as the effective number of participants in the collision process, e_2, and e_4 are the eccentricity related to the harmonics v_2 and v_4 respectively. This set of initial conditions (IC) will be useful in the future to discuss some discrepancies in the results obtained for different nuclei species.

The first observable is presented in figure Figura 13. It represents the p_T distribution for symmetric Au+Au nuclei collisions. This figure was obtained using the set of parameters for Au nuclei obtained by the minimization of $T_R ENT_O$ parameters expressed in table 3, we also use $\kappa_t = 67.4$, $T_f o = 144$. Those first results include the use of FO-EoS, with the number of events (NE) equal to 1000. One can see the reasonable description of particle distribution according to experimental data in all p_T range.

Figura 13 – Au+Au transversal momentum distribution for symmetric nuclei

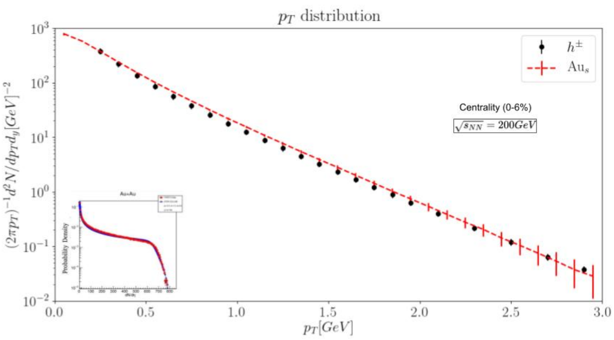

Font: Author's production.

Now aiming to our main goals, observe the effect of deformation in the collective flow, we did several simulations related to the gold nuclei doing a variation in the deformation factors β_2, and β_4. We will present the comparison between the symmetric nuclei, the original deformed nuclei implemented by T_RENT_O and one degree of deformation, a nuclei with β_2 preserved, and β_4 null.

We maintain the same set of T_RENT_O input parameters, use $\kappa_t = 67.4$, and $T_fo = 144$ for the full deformed nuclei $Au_d(\beta_2, \beta_4)$, but we changed the values of κ_t, and T_fo, to 44.2, and 140 respectively for $Au_d(\beta_2)$ nuclei. This modification was necessary due to necessity to reproduce the experimental data for particle distribution, in fact, when we have the initial geometry subjected only to the β_2 parameter it changes the multiplicity.

For deformed gold collisions we have the following initial conditions for Au$_d(\beta_2, \beta_4)$ in table 5:

Tabela 5 – Deformed Au(β_2, β_4)+Au(β_2, β_4) collisions initial conditions

b	9.890
N_{part}	105
e_2	0.427
e_4	0.352

Font: Author's production.

Table 6 show to us the initial conditions for Au$_d(\beta_2)$ collisions in table :

Tabela 6 – Deformed Au(β_2)+Au(β_2) collisions initial conditions

b	9.983
N_{part}	101
e_2	0.438
e_4	0.347

Font: Author's production.

We can see that the deformation factors, or the change of the initial geometry didn't modify roughly the initial conditions for Au nuclei.

The comparison of particle distribution for those nuclei are presented in figure Figura 14.

We can see that the curves almost coincide in all p_T regime for symmetric and full deformed nuclei, looking at the nuclei subjected only to the β_2 factor the values coincide in the the p_T range between $0 < p_T < 1.5$, and split for high p_T regime.

Figura 14 – Au+Au transversal momentum distribution comparison

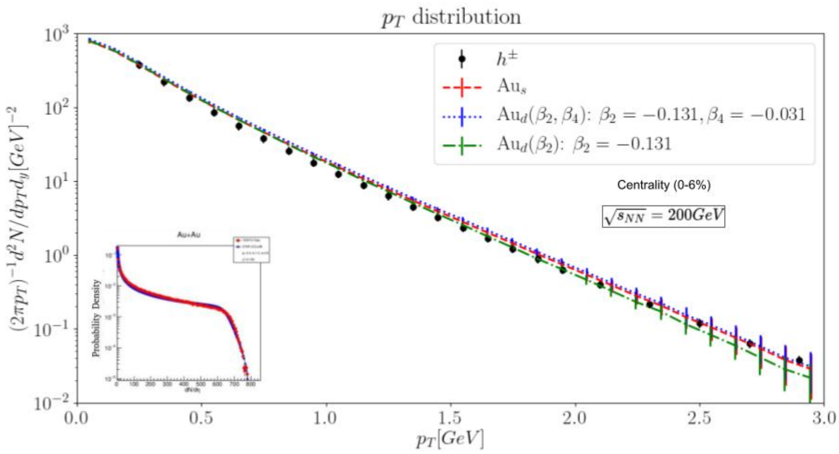

Font: Author's production.

Let us move on to the elliptic flow v_2. The elliptic flow, as we mentioned before, is one of the most important observable in RHIC, because it show to us how the energy is anisotropically distributed. The figure Figura 15 shown to us the results of this set of Au nuclei for ideal Hydrodynamics.

Figura 15 – Au+Au elliptic flow comparison

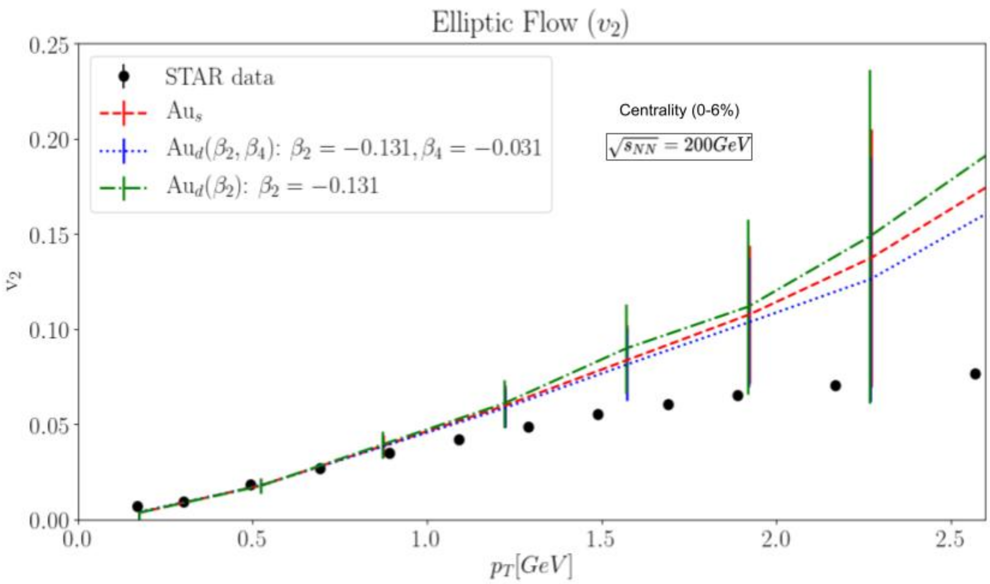

Font: Author's production.

For ideal hydrodynamics, it is expected that the simulations should reproduce the experimental data only for low p_T regime, i.e, for $p_T \leq 1.0MeV$. Once we explicitly claim it, we can see a good acceptance between the simulations and the experimental data in the range mentioned before. The interesting fact to observe is that the v_2 is almost indistinguishable for $p_T \leq 1.2$ approximately.

For high p_T we can observe that deformed nuclei which includes $(\beta_2$, and $\beta 4$ parameters bring the simulation data near to experimental data, i.e, the inclusion of the deformation in this case can be understood as an important tool in the description of v_2. Looking to the Au nuclei subjected to only the β_2 factor we can see a split when compared to the symmetric nuclei and experimental data.

The next result consists in the observation of high harmonics, especially the v_4. Figure Figura 16 presents the comparison between those nuclei for v_4.

Figura 16 – Au+Au v_4 comparison

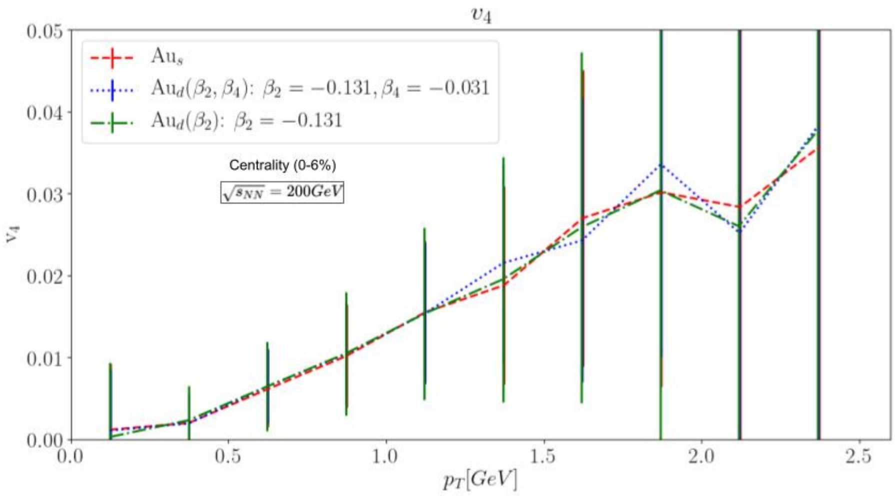

Font: Author's production.

The results for v_4 are almost constant in the p_T regime between $0 < p_T < 1.2$, has a deviation between $p_T > 1.2MeV$. The peaks in $p_T \approx 1.9$, $p_T \approx 2.2$ and $p_T \approx 2.4$ should be considered, once we can see a significantly difference in the peak $p_T \approx 2.2$ for $Au_d(\beta_2)$ and the full deformed and symmetric nuclei. When we look at the local minimum in $p_T \approx 2.2$, both deformed nuclei has the same behavior, while the symmetric nuclei has a higher value.

In order to observe only the effect of the deformation factor β_2, firstly we implement the opposite signal of the deformations factors as one can see in the table 7.

Tabela 7 – Testing a signal variation in Au nuclei

Symbol	β_2	β_4
$Au_d(\beta_2, \beta_4)$	-0.131	-0.031
$Au_d(\beta_2, \beta_4)$	0.131	0.031

Font: Author's production.

We present in Figura 19 express the result of the elliptic flow using the variation expressed in table 7:

The effect of the change of the signal in the deformation factor in Au nuclei induce a deviation between the simulation data comparing to the original signal. This difference become visible for $p_T > 1.3GeV$.

Figura 20 represents the v_4, also using the variation presented in table 7:

A new variation in the deformations parameters was made, in order to see the behavior of the variation of β_2 parameter. The implementations are presented below:

Figura 17 – Au+Au elliptic flow signal comparison

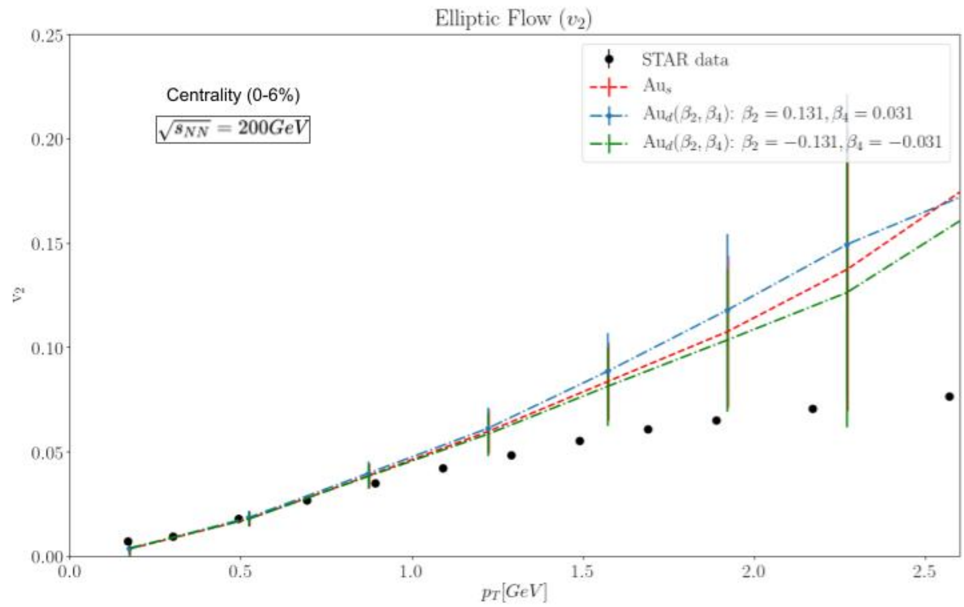

Font: Author's production.

Figura 18 – Au+Au v_4 signal comparison

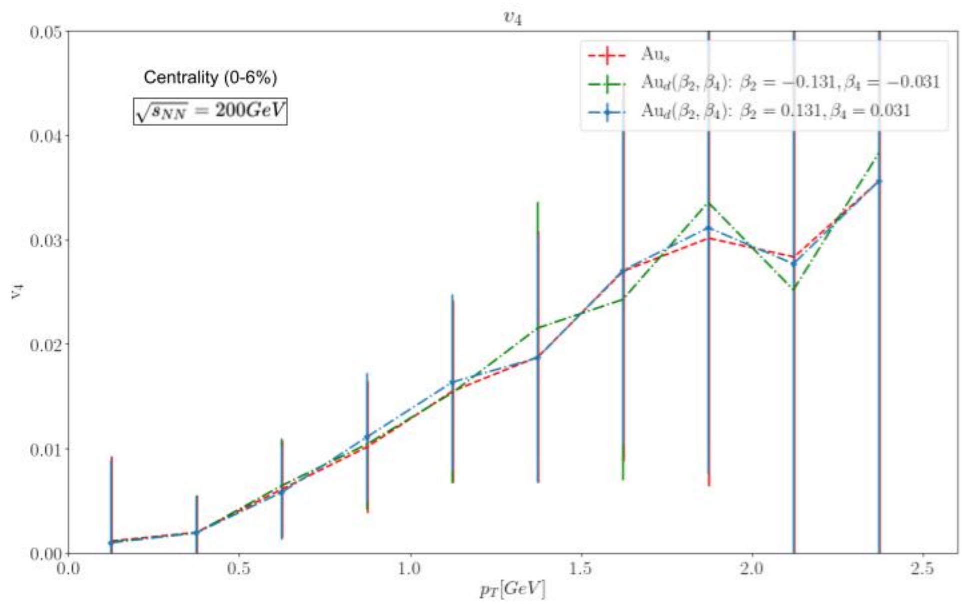

Font: Author's production.

With those degrees of freedom in the β_2 parameter presented in table 8 we obtain the following results for v_2, and v_4:

In Figura 19 we can see that with the systematical increase of deformation factor β_2 we can observe what can be a path to a "linear behavior"of v_2 according to β_2. We cannot make any strong statement

Tabela 8 – β_2 variation in Au nuclei

Symbol	β_2	β_4
$Au_d(\beta_2, \beta_4)$	-0.065	-0.031
$Au_d(\beta_2, \beta_4)$	-0.131	-0.031
$Au_d(\beta_2, \beta_4)$	-0.196	-0.031

Font: Author's production.

Figura 19 – Au+Au v_2 β_2 variation

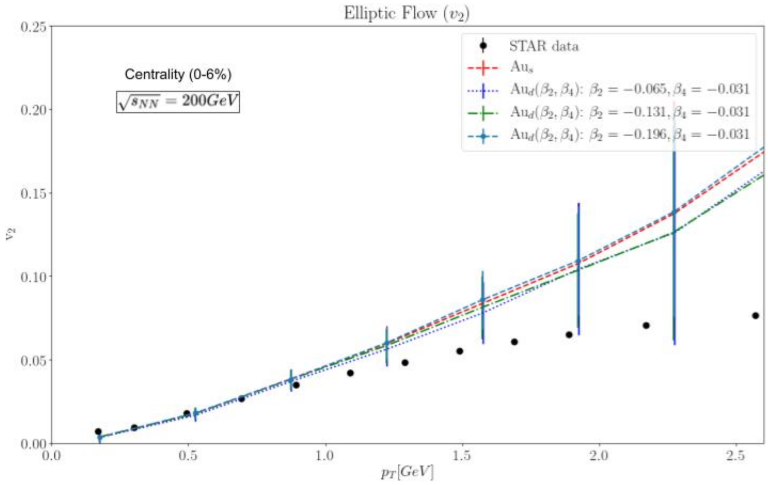

Font: Author's production.

once we still don't have a considerable statistic. Figura 20 is the results regarding the v_4.

Figura 20 – Au+Au v_4 β_2 variation

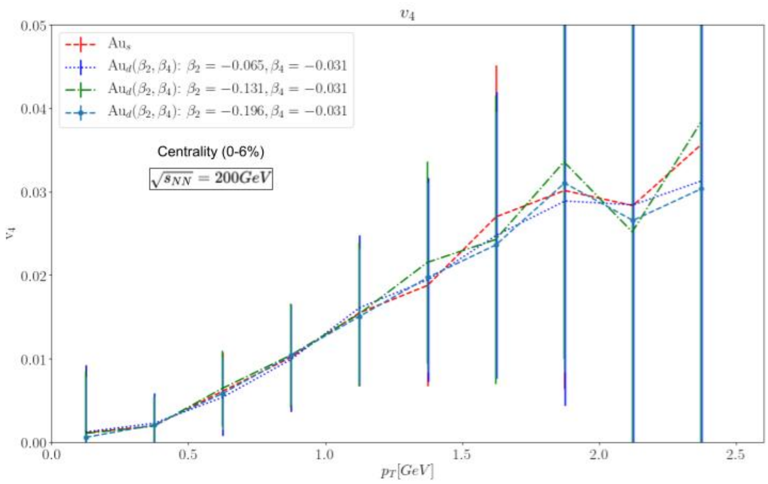

Font: Author's production.

In the next subsection we will present the results related to the Uranium nuclei.

5.1.2 Uranium nuclei

In this subsection we will present our results for uranium nuclei, using the same approach that we used in the Au+Au nuclei collisions. We start showing the initial conditions for symmetric uranium nuclei U_s as follow:

Tabela 9 – Symmetric U+U collisions initial conditions

b	10.976
N_{part}	117
e_2	0.495
e_4	0.442

Font: Author's production.

For deformed nuclei we have the following IC results: And:

Tabela 10 – Deformed U3(β_2, β_4)+U3(β_2, β_4) collisions initial conditions

b	10.052
N_{part}	126
e_2	0.501
e_4	0.440

Font: Author's production.

Tabela 11 – Deformed U2(β_2)+U2(β_2) collisions initial conditions

b	10.159
N_{part}	121
e_2	0.512
e_4	0.447

Font: Author's production.

We easily can see that for all types of U+U collisions, there is a significant change specially in e_2, and e_4 when we compare this data to the data of Au+Au collisions, please see tables 4, 5, and 6.

From now on in this section, we will discuss about the observables. The first result shown in figure Figura 21 and the subsequent, are related to the multiplicity for the first type of symmetric uranium nuclei U_s. For this nuclei we use the set of T_RENT_O input parameters expressed in table 3, for $\kappa_t = 53.3$, $T_{fo} = 145MeV$, and using the FO-EoS.

One can see the multiplicity data can be fitted by our simulation data with reasonable precision all p_T range. Figura 22 represents the multiplicity spectrum including the collisions for symmetric and deformed U nuclei subjected to β_2, and β_4. We can see that the deformation didn't change the multiplicity, resulting in almost the same curves for deformed (red dashed line) and non-deformed (blue dotted line) nuclei.

Figura 23 is the associated elliptic flow v_2 for both simulations:

We can see a visible deviation between the symmetric and deformed nuclei. It is also notable in the high order harmonic v_4 found in Figura 24

Figura 21 – U+U transversal momentum distribution for symmetric nuclei

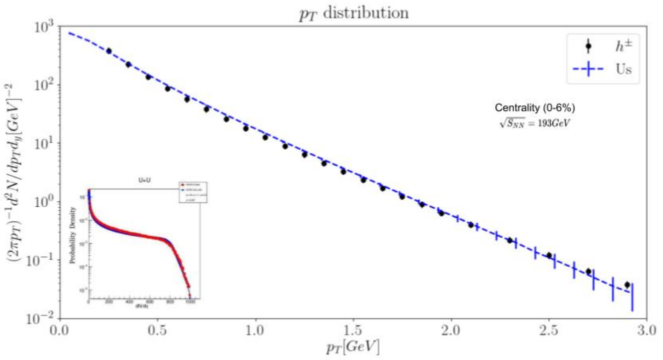

Font: Author's production.

Figura 22 – U+U transversal momentum distribution comparison

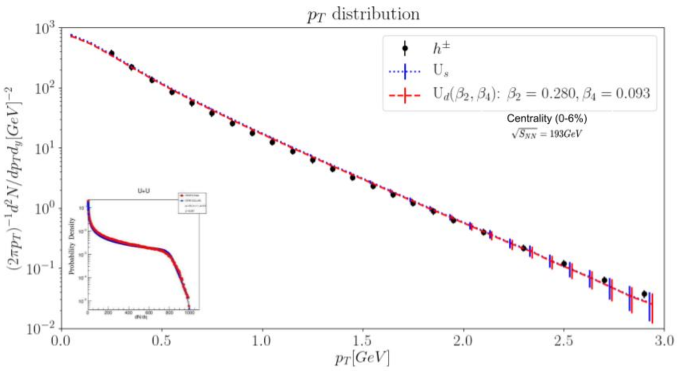

Font: Author's production.

The following results are related to the second and third type of uranium nuclei. The first result presented in figure Figura 25 is related to the multiplicity of symmetric U3+U3 nuclei collisions. For this nuclei we use the freeze-out temperature $T_{fo} = 140MeV$, and $\kappa_t = 49.2$.

In figure Figura 26 we show the results regarding the comparison for deformed, and symmetric nuclei assuming two different degrees of freedom of deformation, one including both deformation factors β_2, β_4 and other using only the β_2 factor. For $U3(\beta_2)$+$U3(\beta_2)$ nuclei collisions, we did a change in T_{fo}, and κ_t in order to fit the multiplicity spectrum. The new values are $T_{fo} = 144MeV$, and $\kappa_t = 52.3$ respectively. In figure Figura 27 we present the elliptic flow:

From figure Figura 27 we have an indication that the absence of β_4 doesn't produce a significant change in data for v_2. Now, looking to the v_4 in figure Figura 28 we can see a more significant deviation between those different U3+U3 nuclei collisions.

Beyond this set of results, as we did in the Au nuclei, we propose a variation in the parameters β_2, β_4. First, we did a change in the signal of the deformation factors as we can see in table 12:

The results of those simulations are presented in figures Figura 29, and Figura 30. The figure Figura 29, show to us a comparison for elliptic flow comparing the effect of the change of signal in the deformation factors. We compare both nuclei present in table 12 against the symmetric one proposed

Figura 23 – U+U elliptic flow comparison

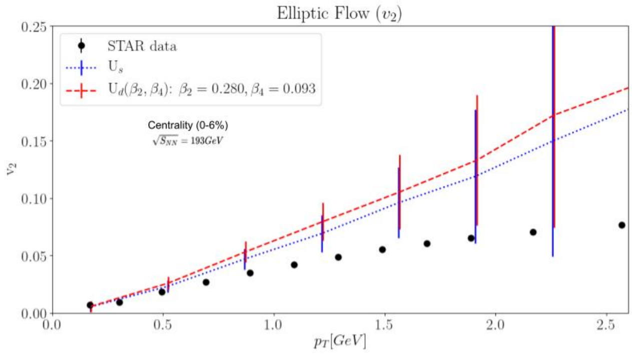

Font: Author's production.

Figura 24 – U+U v_4 comparison

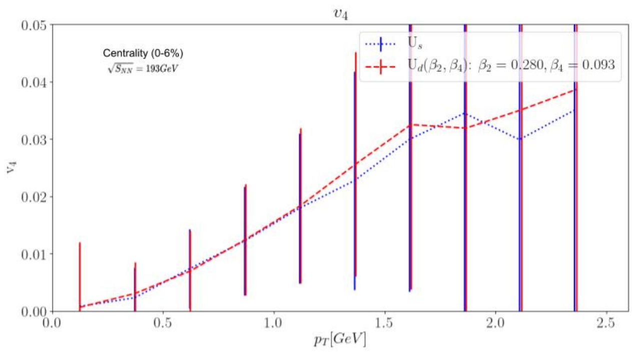

Font: Author's production.

Tabela 12 – Testing a signal variation in U3 nuclei

Symbol	β_2	β_4
$U3_d(\beta_2, \beta_4)$	0.280	0.093
$U3_d(\beta_2, \beta_4)$	-0.280	-0.093

Font: Author's production.

before.

Purple dashed line represents the symmetric U3 nuclei, blue dashed + dotted line represents the negative parameters while the green dotted line is the original deformed nuclei. Using the negative values we can see a better data description in all p_T range. Those results will be confirmed or denied when we increase the number of events in order to obtain smooth curves.

In figure Figura 30 we present the results for the fourth harmonic.

As we did in Au nuclei, we implement a new variation in the β_2 factor, found in table 13

With those variations, we have the following results for elliptic flow, and for v_4 in figures Figura 31, and Figura 32 respectively:

Is important to mention that the effect of statistics. For a more precise results, or smooth curves, we should increase the number of events NE. This can be observed in almost all curves involving the

Figura 25 – U3+U3 transversal momentum distribution for symmetric nuclei

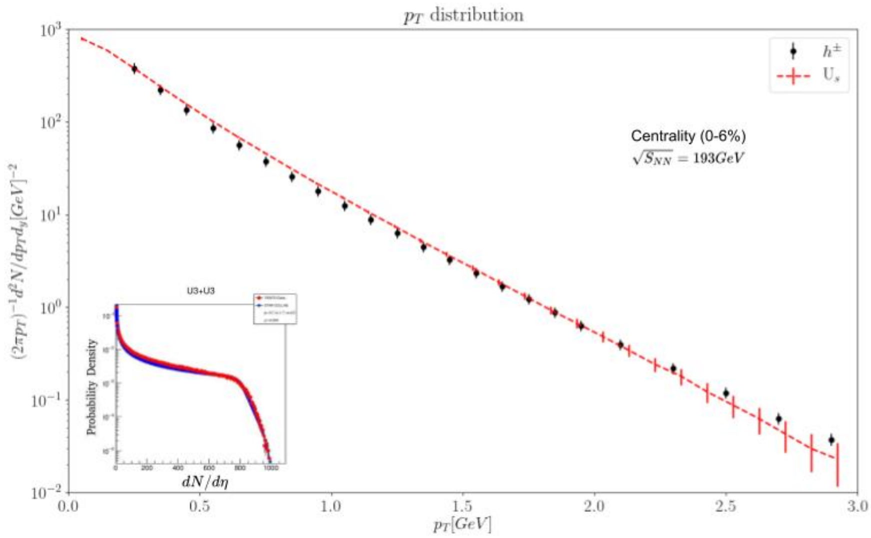

Font: Author’s production.

Figura 26 – U3+U3 transversal momentum distribution comparison

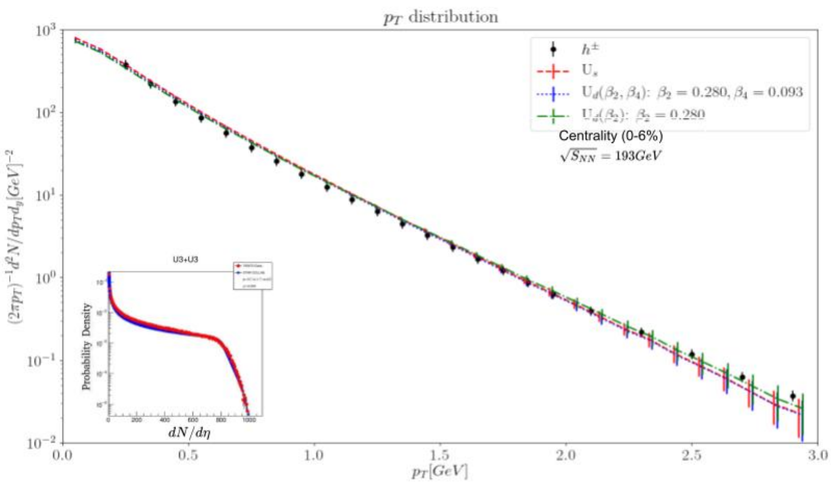

Font: Author’s production.

harmonics, v_2, and v_4. The orange curve for example, representing the harmonic with $\beta_2 = 0.210$, and $\beta_4 = 0.093$ shouldn’t decrease for $2.1 < p_T < 2.4$ for both cases, i.e, both harmonics.

Next section is devoted to present the results including the effect of viscosity for Au and U nuclei.

5.2 VISCOUS HYDRODYNAMICS

In this section we will present the results related to the viscous hydrodynamics. As we mentioned earlier, we expect to have a much more reasonable description, once one of the effects of viscosity is the reduce of pressure and the decrease of the harmonics. We will divide this section in two subsections, one devoted to the presentation of Au+Au nuclei collisions using the HotQCD-EoS, and other to U+U

Figura 27 – U3+U3 elliptic flow comparison

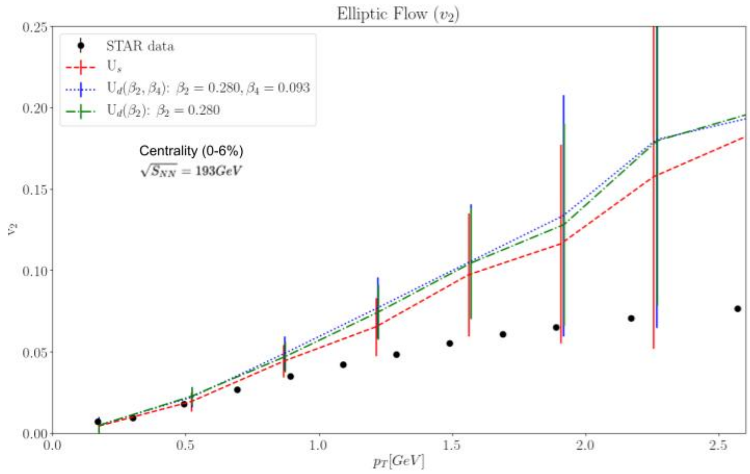

Font: Author’s production.

Figura 28 – U3+U3 v_4 comparison

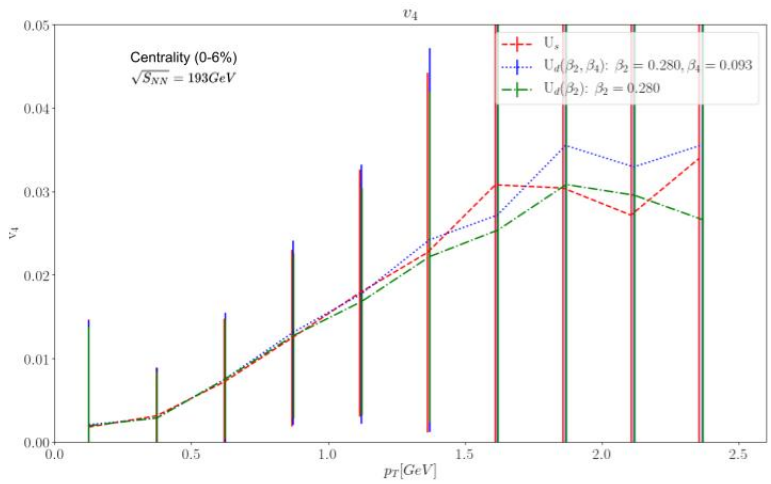

Font: Author’s production.

nuclei using the HotQCD-EoS, and FO-EoS.

5.2.1 Gold Nuclei

For Au+Au nuclei collisions, using the HotQCD-EoS, with the same set of $T_R ENT_O$ input parameters, with $\kappa_t = 47.5$, and $T_{fo} = 146 MeV$ we have the following results for $\eta/s = 0.04$, comparing the symmetric and the original deformed nuclei in Figura 33, Figura 34, and Figura 35.

We will start showing the multiplicity spectrum found in Figura 33. Here we compare the symmetric Au nuclei (red dashed line) and full deformed nuclei (green dashed + dotted line).

Again we can see that the effect of initial geometry of nuclei is not observed in the multiplicity spectrum in the case when β_2, and β_4 are used.

Figura 29 – U3+U3 elliptic flow signal comparison

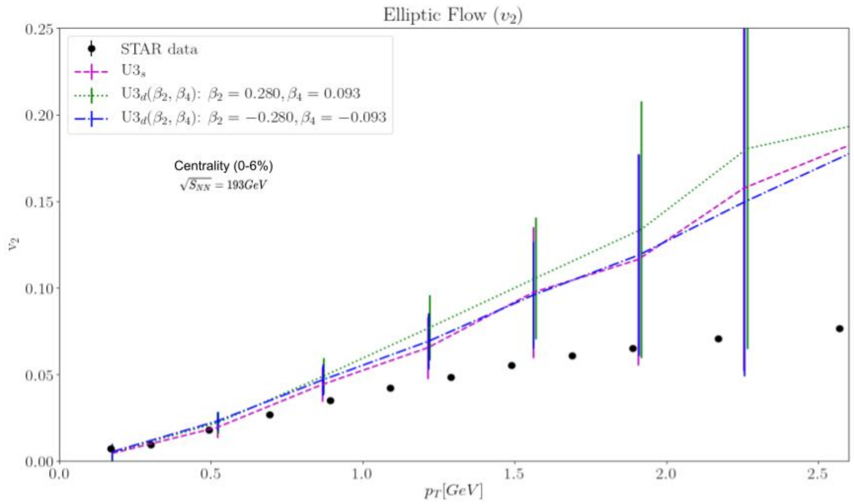

Font: Author's production.

Figura 30 – U3+U3 v_4 signal comparison

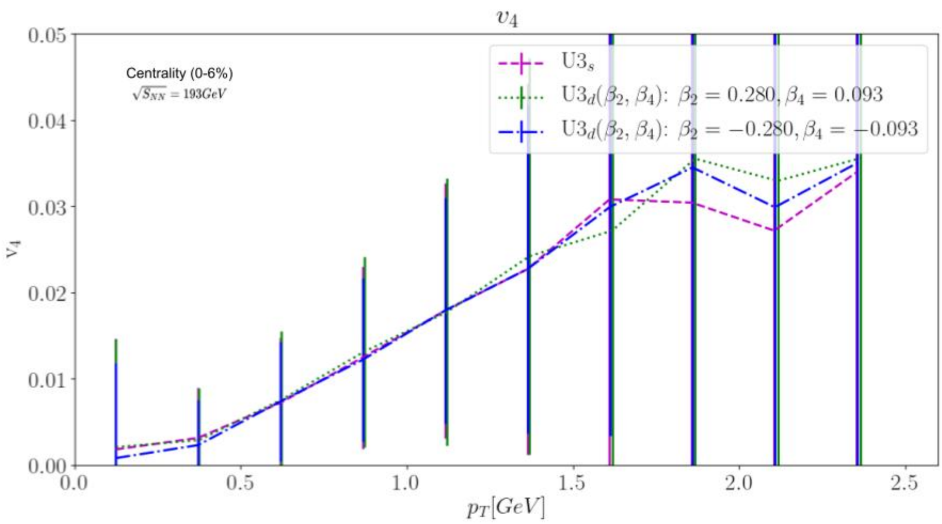

Font: Author's production.

In figure Figura 34 we present the related elliptic flow for both nuclei. Also for HotQCD-EoS we see the same behavior found in FO-EoS for Au nuclei, the deformation factors being useful in order to have a more precise description of data. For high order harmonic v_4 found in figure Figura 35, we can observe also the same behavior as we noticed in results for FO-EoS.

Now we will present some results related to the increase of the value of shear the viscosity. We keep the same set of T_{fo}, κ_t, and T_RENT_O input parameters. Figure Figura 36 is the multiplicity spectrum obtained using $\eta/s = 0.08$.

The associated elliptic flow can be found in figure Figura 37.

One can see, using high values of shear viscosity η/s we can have a better data description. In figure Figura 38 we present the v_4 as follow:

In next subsection we will present some results related to viscous hydrodynamics for uranium

Tabela 13 – Testing a β_2 variation in U3 nuclei

Symbol	β_2	β_4
$U3_d(\beta_2, \beta_4)$	0.070	0.093
$U3_d(\beta_2, \beta_4)$	0.140	0.093
$U3_d(\beta_2, \beta_4)$	0.210	0.093
$U3_d(\beta_2, \beta_4)$	0.280	0.093

Font: Author's production.

Figura 31 – U3+U3 elliptic flow β_2 comparison

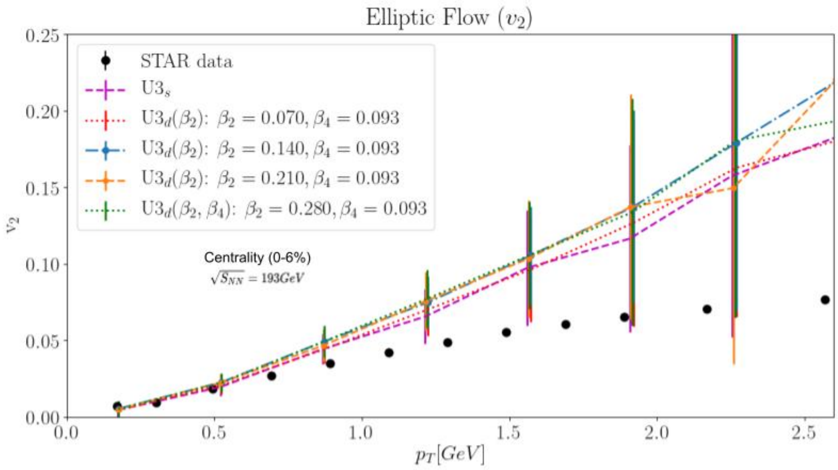

Font: Author's production.

nuclei collisions.

Figura 32 – U3+U3 v_4 β_2 comparison

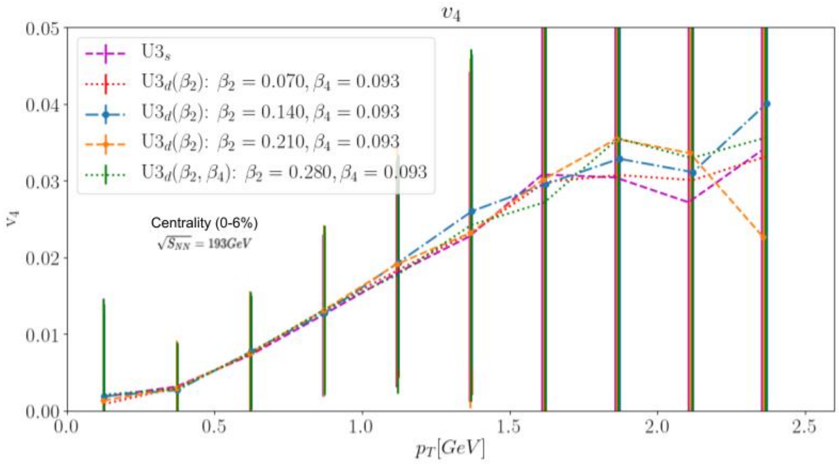

Font: Author's production.

Figura 33 – Au+Au transversal momentum distribution for HotQCD: $\eta/s = 0.04$

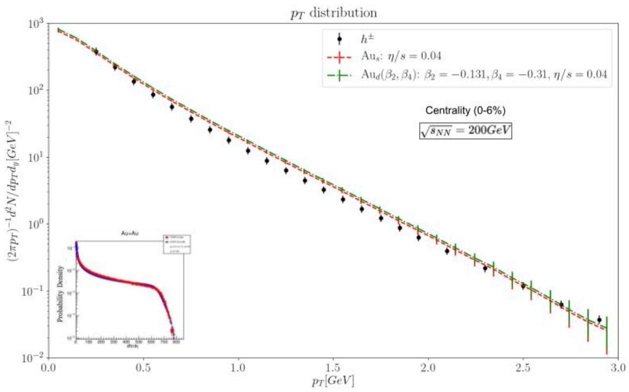

Font: Author's production.

5.2.2 U Nuclei

For the uranium nuclei collisions we will start comparing the results for the viscous hydrodynamics using the FO-EoS. We compare the results that we have for collisons of U3s+U3s ideal hydrodynamics and include a small viscosity, $\eta/s = 0.04$, assuming the same set of parameters, including the κ_t, and T_{fo} already presented. Figura 39 is the comparison for multiplicity spectrum for both cases, the ideal and viscous.

It is easy to see that the viscosity doesn't play an a significant change in the curve in the low p_T regime. If we look at the high p_T regime, the viscosity will change affect the curve, and it will be much more clear when we look at the harmonics, in Figura 40, and Figura 41.

The effect of viscosity can be observed in both harmonics, v_2, and v_4. For v_2 we an see the curves become to split for $p_T \approx 0.7GeV$, with the curve obtained by viscous hydrodynamics becoming a more reasonable description. It is important to mention the fact that $\eta/s = 0.04$ is a small value, and still is considered as ideal case.

Figura 34 – Au+Au elliptic flow for HotQCD: $\eta/s = 0.04$

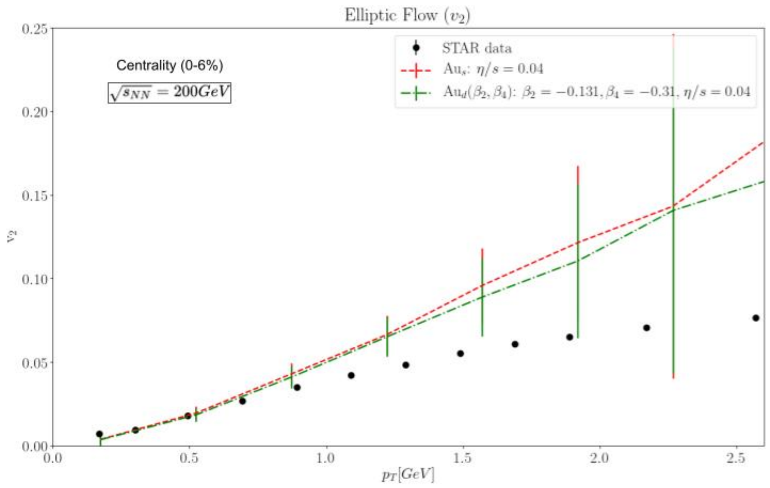

Font: Author's production.

Figura 35 – Au+Au v_4 for HotQCD: $\eta/s = 0.04$

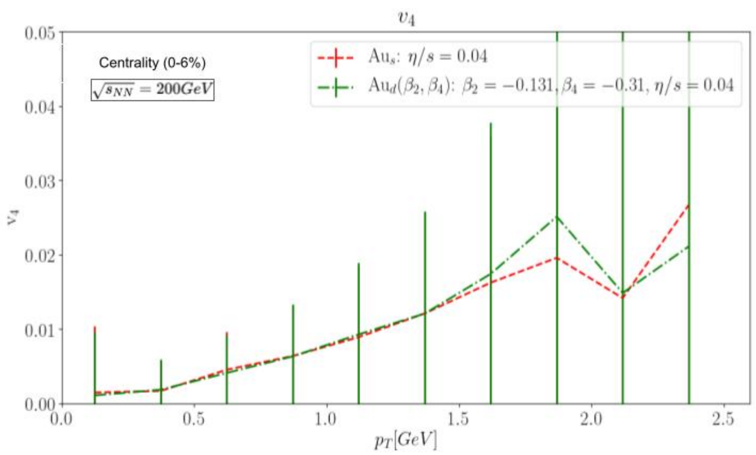

Font: Author's production.

Even though using this small value of η/s, the effect of viscosity can be observed especially in the high harmonic v_4. There is a difference between the curves in v_4 harmonic almost in all p_T regime.

Now, we will present the results for U3+U3 collisions using the HotQCD-EoS. The first result is presented in figure Figura 42, which represents the multiplicity for the symmetric U3 nuclei. We use for this simulations the shear viscosity $\eta/s = 0.04$.

The elliptic flow is presented in figure Figura 43:

The v_4 can be found in the figure Figura 47:

The following results is related to U2+U2 nuclei, dependent of β_2 only. For this nuclei we use $T_{fo} = 151MeV$, and $\kappa_t = 45.9$. Figure Figura 45 is the multiplicity.

The elliptic flow is presented in figure Figura 46:

Figura 36 – Au+Au transversal momentum distribution

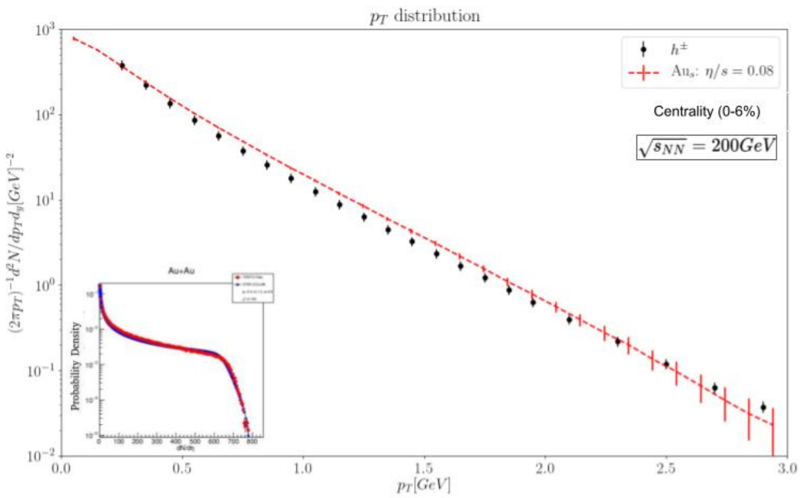

Font: Author's production.

Figura 37 – Au+Au elliptic flow

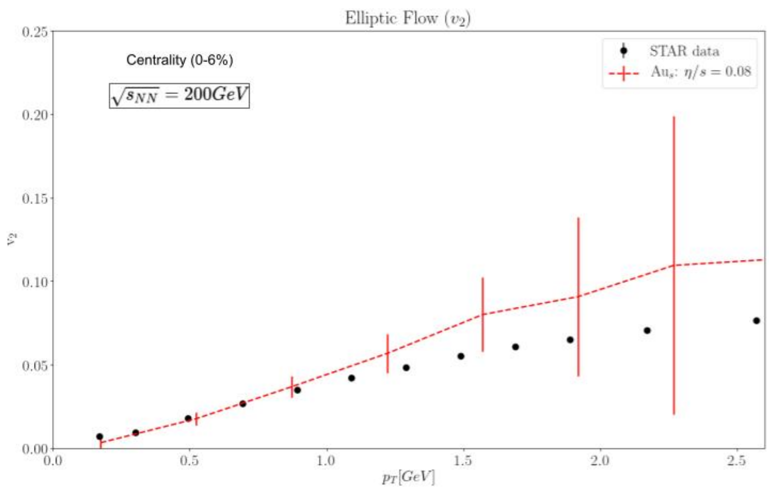

Font: Author's production.

The v_4 can be found in the figure Figura 47:

Finally we will show the results for U3+U3 collisions with dependence of β_2, and β_4 parameters. Figure Figura 48 is the multiplicity.

After presenting each uranium nuclei separately for HotQCD-EoS, we will compare all those results. The first comparison is expressed in the multiplicity spectrum in figure Figura 51.

The elliptic flow is presented in figure Figura 52:

v_4 is presented in figure Figura 53

Figura 38 – Au+Au v_4

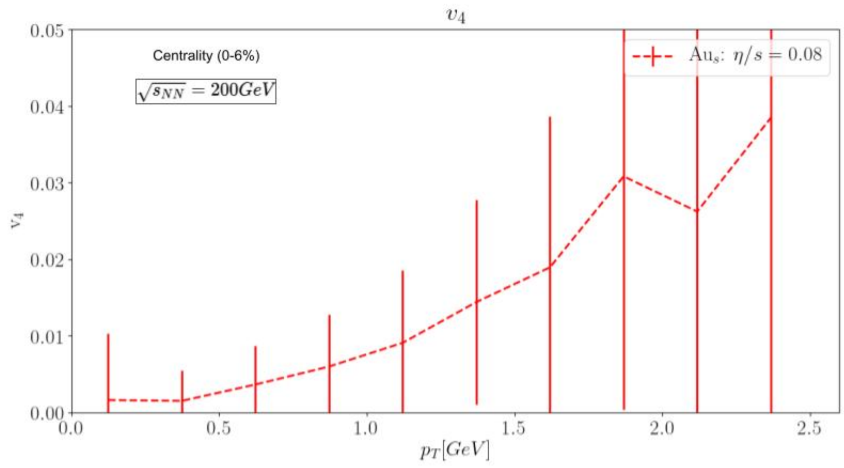

Font: Author's production.

Figura 39 – U3s+U3s transversal momentum distribution comparison with viscosity

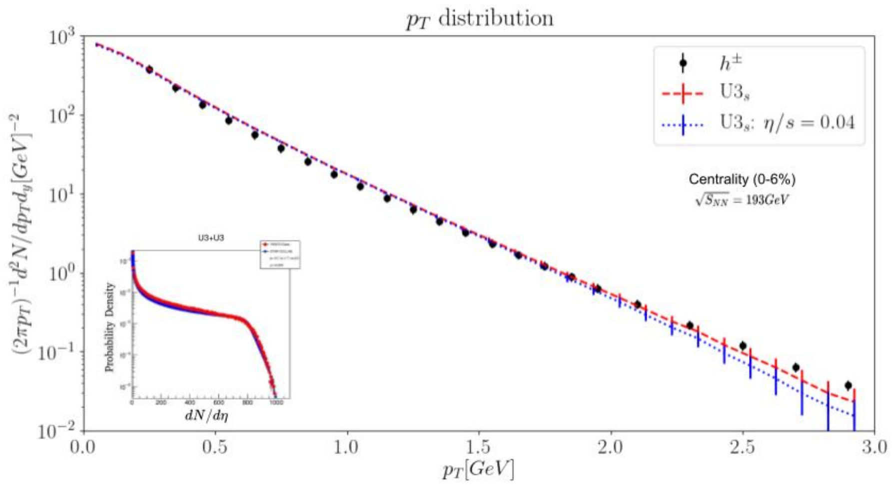

Font: Author's production.

5.3 EOS COMPARISON

In this final section, we will present a comparison between both EoS presented. In Figura 54 we have the results for U3s+U3s collisions, comparing the multiplicity spectrum for both EoS. The cyan dashed line is related the FO-EoS, while purple line regards the results of HotQCD-EoS. In both cases we assume a shear viscosity $\eta/s = 0.04$.

We can see for multiplicity spectrum, the FO-EoS has a better description for low p_T regime, while HotQCD-EoS has a better description for high p_T regime. Now, looking at the collective flow we will see a significant difference, specially for v_2.

The elliptic flow v_2 is presented in Figura 55. We can see that for $p_T < 0.8GeV$ both EoS's have a reasonable description. After this region, the results for FO-EoS and HotQCD-EoS split, and FO-EoS

Figura 40 – U3s+U3s elliptic flow comparison with viscosity

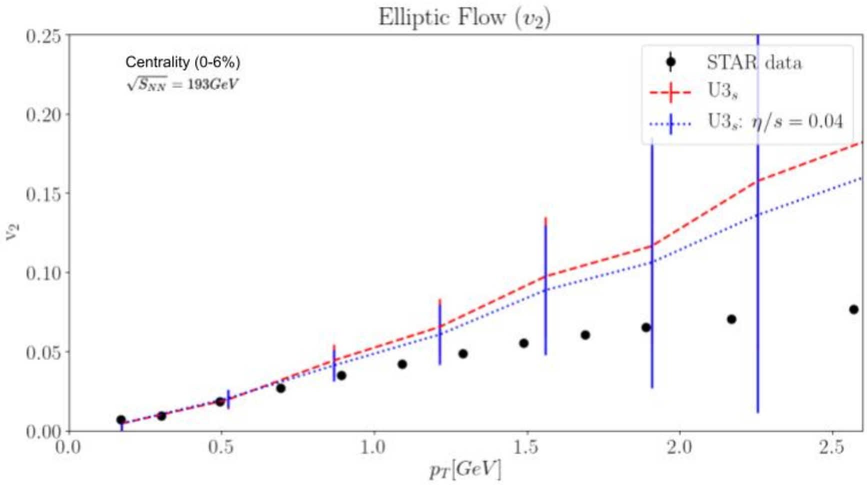

Font: Author's production.

Figura 41 – U3+U3 v_4 comparison with viscosity

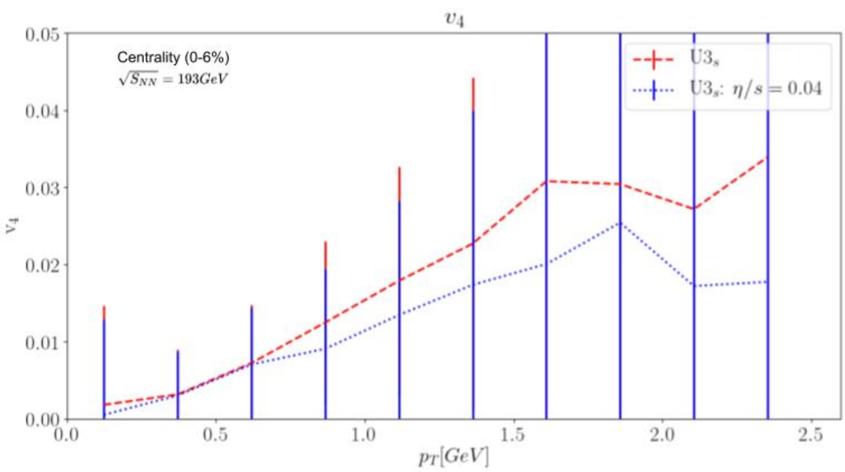

Font: Author's production.

seems a better description. We still need to consider the fact that we are in ideal case, $\eta/s = 0.04$.

The last result is the v_4, presented in Figura 56.

In the final chapter of this work we will cast some important points still not argued.

Figura 42 – Us+Us transversal momentum distribution for HotQCD-EoS

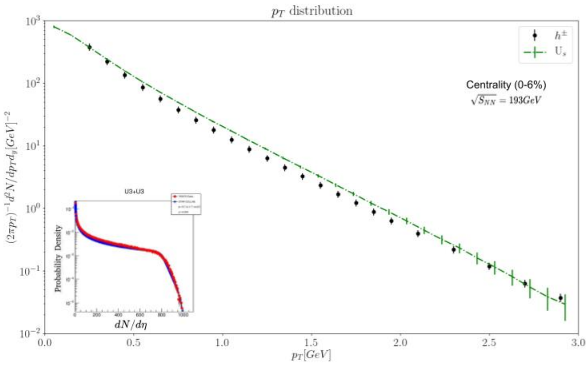

Font: Author's production.

Figura 43 – U3+U3 elliptic flow for HotQCD-EoS

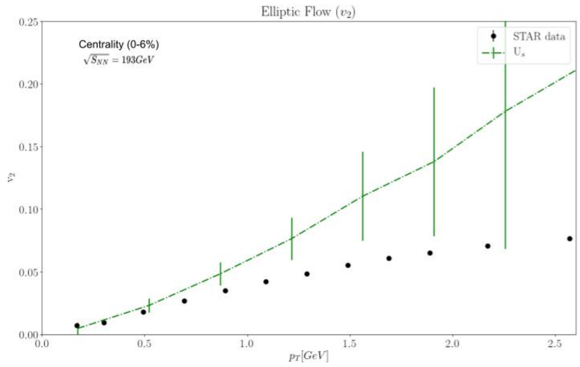

Font: Author's production.

Figura 44 – U3+U3 v_4 for HotQCD-EoS

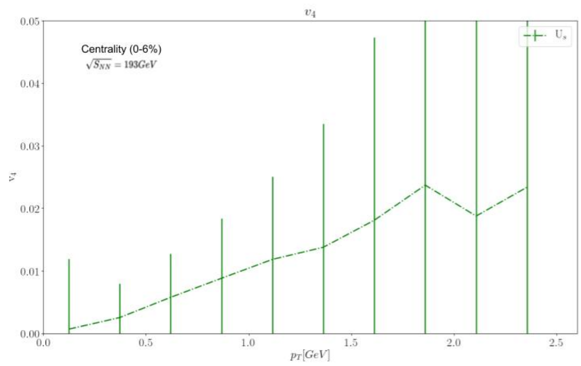

Font: Author's production.

Figura 45 – U2+U2 transversal momentum distribution for HotQCD-EoS

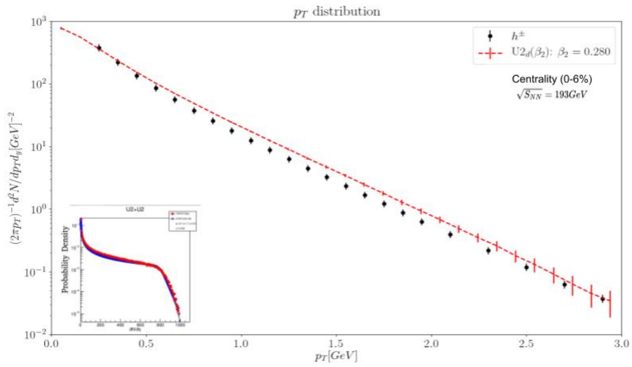

Font: Author's production.

Figura 46 – U2+U2 elliptic flow for HotQCD-EoS

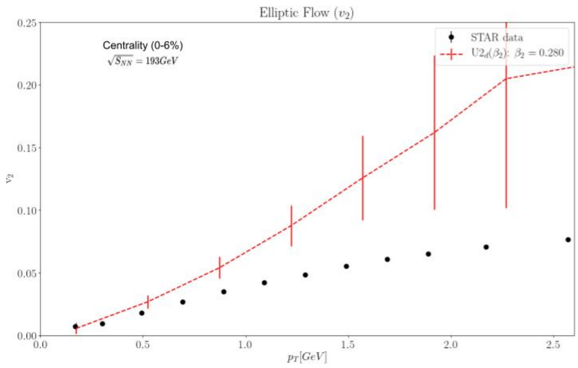

Font: Author's production.

Figura 47 – U3+U3 v_4 for HotQCD-EoS

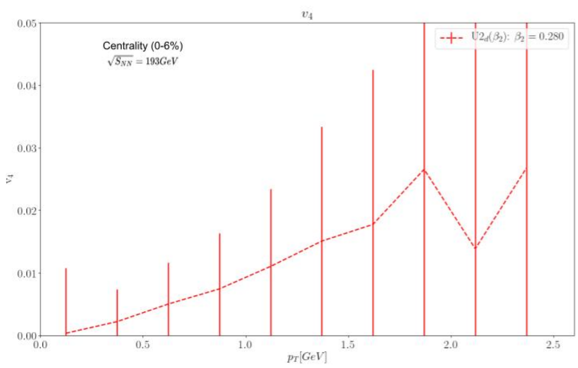

Font: Author's production.

Figura 48 – U3+U3 transversal momentum distribution for HotQCD-EoS

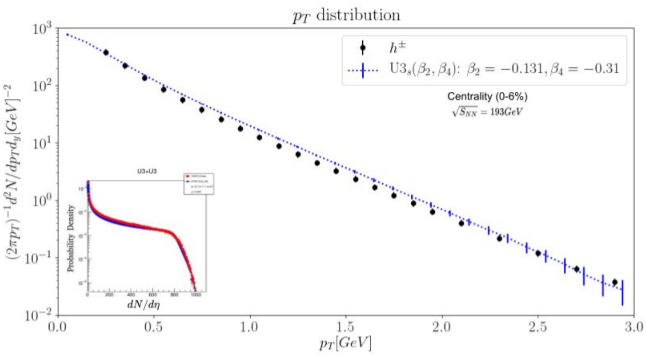

Font: Author's production.

Figura 49 – U3+U3 elliptic flow for HotQCD-EoS

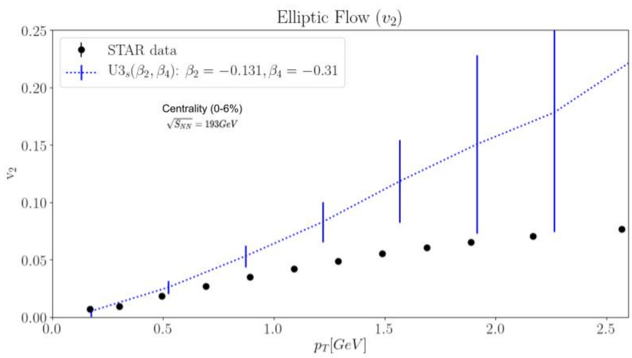

Font: Author's production.

Figura 50 – U3+U3 v_4 for HotQCD-EoS

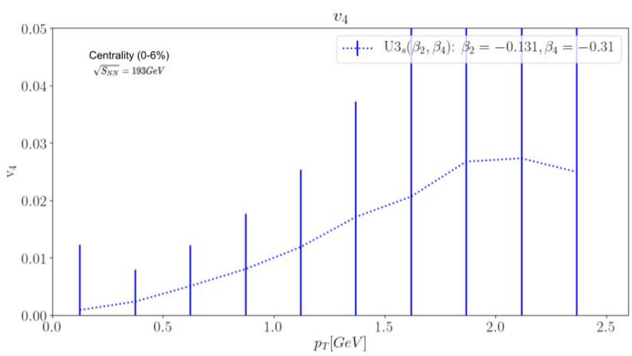

Font: Author's production.

Figura 51 – Uranium transversal momentum distribution deformation comparison for HotQCD-EoS

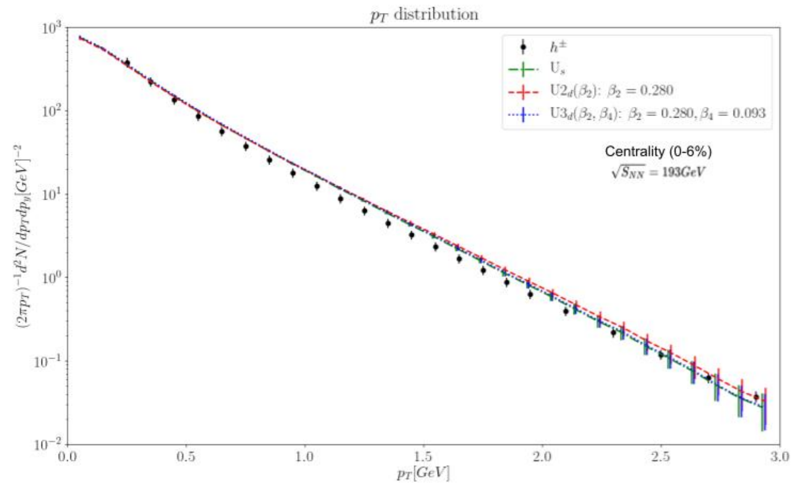

Font: Author's production.

Figura 52 – Uranium elliptic flow comparison for HotQCD-EoS

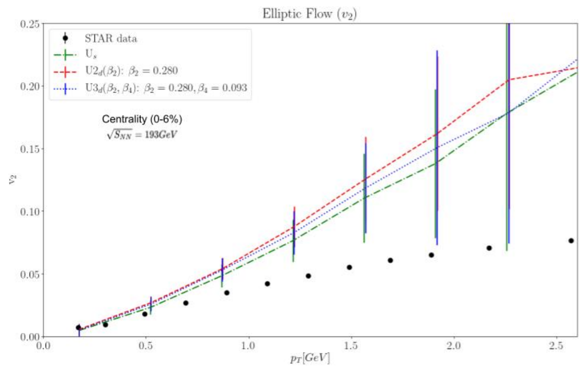

Font: Author's production.

Figura 53 – Uranium v_4 comparison for HotQCD-EoS

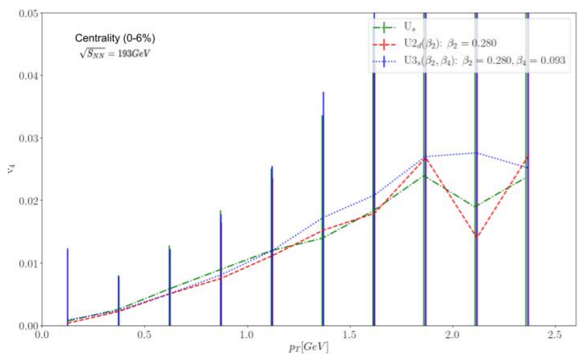

Font: Author's production.

Figura 54 – U3s+U3s transversal momentum distribution comparison with viscosity

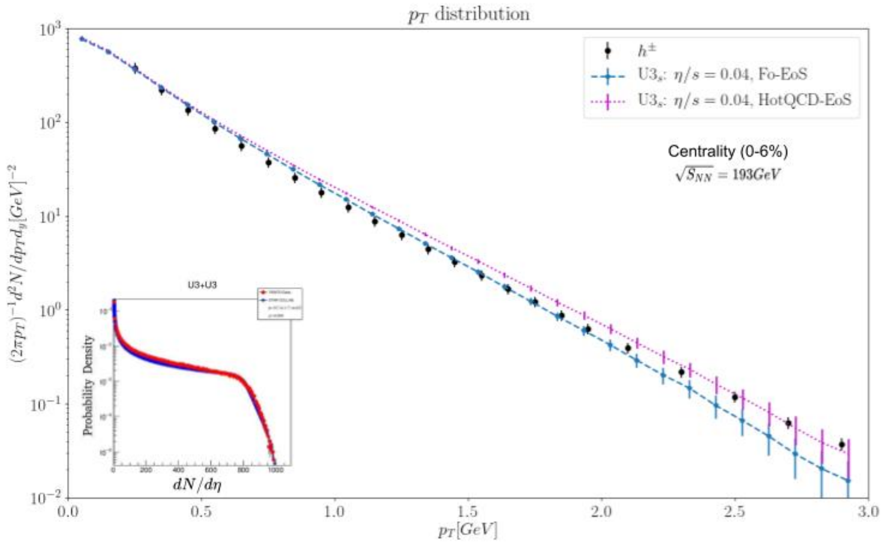

Font: Author's production.

Figura 55 – U3s+U3s elliptic flow comparison with viscosity

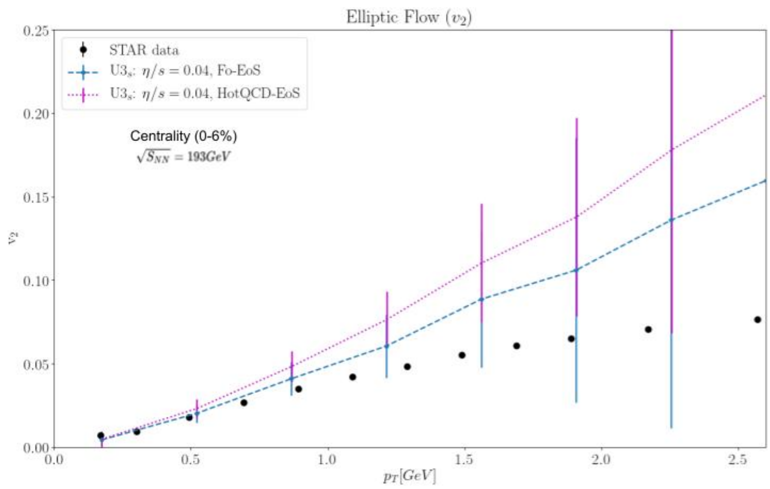

Font: Author's production.

Figura 56 – U3s+U3s v_4 comparison with viscosity

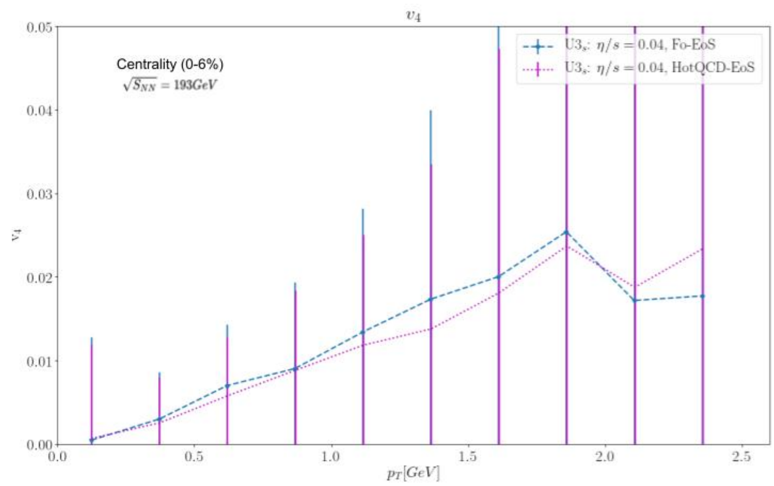

Font: Author’s production.

6 CONCLUSIONS

In chapter 1 we introduce the theory used to accomplish our aim, a theoretical study involving numerical simulations to observe the effect of deformed nuclei in hydrodynamic evolution and the final observables. Chapter 2 was devoted to present the theory used in the scope of our studies, passing through all stages in relativistic heavy ion collisions, the initial conditions based on the collision process, the space-time evolution described by the implementation of relativistic hydrodynamics, and the decoupling stage, where the direct hadrons decay and can freely travel and be identified in the detectors.

We presented the Glauber model to describe the collision process, which is an optical model used to obtain quantities such as the impact parameter b, the number of participants N_{part}, and the eccentricity, which give to us the spatial anisotropy. The relativistic hydrodinamics theory was introduced in order to present the equations of motion, i.e, the system space-time evolution. We present ideal as well viscous hydrodynamics, showing the effect of the viscosity in the energy-momentum tensor, charge-current, and equations of motion. We also present in chapter 2 the Cooper-Frye prescription, used to describe the hadrons decoupling.

Another important tool used to complete the space-time evolution is the equation of state (EoS). With a capable EoS, one can close, and relate the relations such as temperature, pressure, etc. We presented two EoS, the first-order (FO-EoS), composed by the quark-gluon plasm (QGP) and the hadron gas (HG), as well as the HotQCD-EoS, which assumes a mix of relations for pressure, and temperature for high or low temperature regime.

In chapter 4 we focous on numerical implementation, using the theory addressed in chapter 2. Also we present the CHESS code, a script which includes all stages of relativistic heavy ion collisions, based on three well-know codes, T_RENT_O, VHLLE, and THERMINATOR 2, as well as some modifications that we made.

Using the CHESS code we reached the results present in chapter 5. Firstly, we show the original nuclei implemented in T_RENT_O, and had started showing the behavior of the woods-saxon perfil under the effect of deformation factors. Figures Figura 8, Figura 9, Figura 10, and Figura 11 are related the results of our implementation of woods-saxon perfil via ROOT. For Au nuclei, the deformation factors doesn't play a significant change in the perfil when compared to symmetric nuclei, on the other hand, for all nuclei types we have a visible deviation between symmetric and deformed nuclei. The difference between uranium nuclei are due to the variation of deformations factors, which is a higher value when compared to Au nuclei, but also due to geometric parameters, R, and a.

We present a new set of nuclei, which was implemented in T_RENT_O by hand, and showed in the table 2. We also did a minimization of T_RENT_O input parameters, in order to obtain a set of parameters $p, k,$ and w which minimizes the χ^2-test, based on STAR collaboration data proposed in (ADAMCZYK,). The minimized set of T_RENT_O input parameters was present in table 3, and results for χ^2-test can be found it figure **??**.

With this set of parameters, we did a search to a relation for the scale parameter κ_t, and freeze-out temperature T_{fo} to finally obtain the final observables and compare the effect of deformation factor in the collective flow. In section 5.1 we present the results for ideal hydrodynamics, using the FO-EoS for gold and uranium nuclei.

The first result obtained was the initial conditions for symmetric Au+Au nuclei collisions, available in table 4. The particle distribution for symmetric Au+Au nuclei collisions can be found in figure Figura 13. The subsequent results are related to deformed gold nuclei collisions, where we use two different nuclei, assuming in one nuclei the dependence of β_2, β_4 parameters, and one dependence of β_2 only. For the deformed gold nuclei with dependence of β_2, β_4 parameters the relation for κ_t, and T_{fo} was unchanged, while for nuclei which depends to β_2 only, the κ_t, and T_{fo} needed to be changed, in order to fit the particle distribution.

In other words, when we have the loss of symmetry in the nuclei initial geometry, it affect the multiplicity. The values for T_{fo}, and κ_t decrease. We present in tables 5, and 6 the IC for deformed nuclei. The set of IC didn't differs significantly when we compare symmetric and deformed nuclei. The comparison between the observables for those set of nuclei can be found in figures Figura 14, Figura 15, and Figura 16.

The full deformed nuclei, i.e, dependent of both deformation factors seems to be a more reasonable description to experimental data, while one parameter dependence seems to split the simulation data to experimental data, for v_2. We must clarify also the fact that our simulation still don't have enough statistic to reproduce smooth curves for harmonics.

We proposed a variation in the signal of deformation factors to evaluate the behavior under this variation, we can see in figure Figura 19 that this variation also increase the v_2, and causes a split when compared to experimental data and the original deformation parameters.

We also proposed beyond this variation in the signal of deformation factors, a variation in the values of deformation factor β_2, keeping β_4 unchanged according to table 8. In figure Figura 19 we can see what seems some linear behavior in the relation v_2 and β_2. If the β_2 assume a small value, it has a asymptotic behavior, tending to the values assumed by symmetric nuclei. If β_2 assumes values higher then the original one, it seems to be even a better description of experimental data.

We did the same approach for uranium simulations, firstly using the FO-EoS. For U+U nuclei collisions, one can find in elliptic flow v_2 in figure Figura 23 that the deformation induces a deviation from experimental data, and from symmetric nuclei. It was also observed for U3+U3 nuclei, figure Figura 27. For the variation in the parameters signal, we shown in figure Figura 29 that maybe it can be a more reasonable description.

The variation in the β_2 factor according to table 13, also show to us some linear behavior in the relation v_2, β_2. Small values of β_2 induces an approximation of symmetric nuclei data, while higher values split it.

In section 5.2 we present some results for FO-EoS, and HotQCD-EoS using the viscous hydrodynamics for Au+Au and U+U collisions. Specially in harmonics, such as found in figures Figura 34, Figura 35, Figura 37, Figura 38 for Au+Au collisions, and Figura 40, Figura 41, Figura 52, and Figura 53 for U+U nuclei, we can clearly see how the viscosity is important to decrease the values of harmonics due to reduction of pressure.

In section 5.3 we present a comparison between the two EoS used, the FO-EoS and HotQCD. We can see for multiplicity presented in figure Figura 54, the HotQCD-EoS describes better the data, but when we compare the v_2 the FO-EoS seems a more reasonable description for experimental data, while for v_4 both curves are quite similar in the peaks.

We conclude our work without any strong claim, once we still don't have enough statistic, i.e, the number of events used still are not enough to produce a smooth curves for high harmonics. Also, the deformation seems to be a good ally to describe the experimental data for v_2 in Au+Au collisions, while for original uranium nuclei types implemented in T_RENT_O deviates the results. One can use some authors such as Giacalone (GIACALONE,) to explain this fact due to eccentricity and v_2 cumulants, assuming that the relation $v_2\{2\} = \kappa\, e_2\{2\}$ is valid. It is reasonable according to our results, once we show that e_2, and e_4 assume higher values for uranium collisions.

The next steep of this study will be consisted to continue this systematic study of deformation parameters, in principle we will increase the number of events, and after that we also will implement a variation in β_4, keeping β_2 unchanged to also check the behavior of this variation in collective flow.

REFERÊNCIAS

ADAMCZYK, L. E. a. Azimuthal anisotropy in u+u and au+au collisions at rhic. **Phys. Rev. Lett.**, v. 115, n. 222301.

B. SHEN C., T. P. S. Features of the ip-glasma. **Nuclear Physics A**.

BHALERAO, R. Relativistic heavy-ion collisions. **CERN**.

BHALERAOA RAJEEV S. OLLITRAUL, J.-Y. Eccentricity fluctuations and elliptic flow at rhic. **Physics Letters B**, v. 641, n. 3, p. 260–264, 2006.

CHODOS R. L. JAFFE, K. J. C. B. T. V. F. W. A. New extended model of hadrons. **Phys. Rev. D**, v. 9, n. 3471.

CHOJNACKI M. LAJ; KISIEL, A. F. W. B. W. Therminator 2: Thermal heavy ion generator 2. **Comput. Phys. Commun.**, v. 183, n. 3, p. 746–773, 2002.

COOPER F. ; FRYE, G. Single-particle distribution in the hydrodynamic and statistical thermodynamic models of multiparticle production. **Phys. Rev. D**, v. 10, n. 186.

COOPER, G. F. F. Single-particle distribution in the hydrodynamic and statistical thermodynamic models of multiparticle production. **Phys. Rev., D**, v. 10, n. 186.

COOPER, G. F. F.; SCHONBERG., E. Landau's hydrodynamic model of particle production and electron-positron annihilation into hadrons. **Phys. Rev., D**, v. 11, n. 192.

FLORKOWSKI W. HELLER, M. P. S. M. New theories of relativistic hydrodynamics in the lhc era. **Reports on Progress in Physics**, v. 81, n. 4.

GATTRINGER, C. B. L. C. **Quantum chromodynamics on the lattice: an introductory presentation**. Berlin Heidelberg, - Germain: Springer-Verlag, 2010.

GELL-MANN, M. A schematic model of baryons and mesons. **Phys. Lett.**, v. 8.

GIACALONE, G. Elliptic flow fluctuations in central collisions of spherical and deformed nuclei. **Phys. Rev. Lett.**, v. 115, n. 222301.

HISCOCK, L. L. W. A. Generic instabilities in first-order dissipative relativistic fluid theories. **Phys. Rev., D**, v. 31, n. 725.

HUOVINEN, P.; PETRECZKY, P. Qcd equation of state and hadron resonance gas. **Nucl. Phys., A**, v. 827, n. 1-2, p. 26–53, 2011.

HUOVINEN P.; BLEICHER, M. K. I. A 3+1 dimensional viscous hydrodynamic code for relativistic heavy ion collisions. **Comput. Phys. Commun.**, v. 185, n. 3016.

ISRAEL, W. S. Transient relativistic thermodynamics and kinetic theory. **Annals of Physics**, v. 118, n. 341, p. 341–372, 1979.

LANDAU L. D., L. E. M. **Fluid Mechanics**. [S.l.]: Pergamon, 1958.

LATTES C. M. G. ; MUIRHEAD, H. . O. G. P. S. P. C. F. Processes involving charged mesons. **Nature**.

MAKI, M. N. Z.; SAKATA., S. Remarks on the unified model of elementary particles. **Prog. Theor. Phys.**, v. 28, n. 5, p. 870–880, 1962.

MAKI M. NAKAGAWA, Y. O. Z.; SAKATA., S. A unified model for elementary particles. **Prog. Theor. Phys.**, v. 23, n. 1174, p. 1174–1180, 1960.

MILLER M. L.; REYGERS, K.; SANDERS STEPHEN, J. S. P. Glauber modeling in high-energy nuclear collisions. **Annual Review of Nuclear and Particle Science**, v. 57, n. 1, p. 205–243, 2007.

MORELAND J. C.; BERNHARD, J. E. B. S. A. Alternative ansatz to wounded nucleon and binary collision scaling in high-energy nuclear collisions. **Physical Review C**, v. 92, n. 1.

MULLER, I. Zum paradoxon der wärmeleitungstheorie. **Zeitschrift für Physik**, v. 198, n. 4, p. 329–344, 1967.

MURONGA, A. Viscous hydrodynamics. **Strangeness in quark matter. Proceedings**.

RAFELSKI, J. Discovery of quark-gluon plasma: Strangeness diaries. **The European Physical Journal Special Topiscs**.

RAMALLO, A. V. Introduction to the ads/cft correspondence. **Lectures on Particle Physics, Astrophysics and Cosmology**.

SAKATA, S. On a composite model for the new particles. **Prog. Theor. Phys.**, v. 16, n. 686, p. 686–688, 1956.

SHOU Q.Y; MA, Y. S. P. T. A. V. F. W. H. Parametrization of deformed nuclei for glauber modeling in relativistic heavy ion collisions. **Phsysics letters B**, v. 749.

SMELLINGS, R. Elliptic flow: a brief review. **New Journal of Physics**, v. 13, n. 055008.

SOUZA R. D. KOIDE, T. K. T. Hydrodynamic approaches in relativistic heavy ion reactions. **Prog.Part.Nucl.Phys.**, v. 86.

TEANEY, D.; YAN, L. Triangularity and dipole asymmetry in relativistic heavy ion collisions. **Phys. Rev. C**, v. 83, n. 064904.

YEN M. I. GORENSTEIN, W. G. S.-N. Y. G. D. Excluded volume hadron gas model for particle number ratios in a+a collisions. **Phys. Rev., C**, v. 56, n. 2217.

ZWEIG, G. Developments in the quark theory of hadrons. **CERN**, v. 1, n. 22, p. 22–101, 1964.